

KU-16-1
**Determination of Fatigue Resistance of Coupler
Connections in Aluminum Overhead Truss Structures**

By

Danqing Yu, M.S.

Caroline Bennett, Ph.D., P.E.

Jian Li, Ph.D., P.E.

William Collins, Ph.D., P.E.

Elaina Sutley, Ph.D.

A Report on Research Sponsored by
The Kansas Department of Transportation

Structural Engineering and Engineering Materials
SM Report No. 137
August 2020



THE UNIVERSITY OF KANSAS CENTER FOR RESEARCH, INC.

2385 Irving Hill Road – Campus West, Lawrence, Kansas 66045

Executive Summary

Overhead truss sign structures (OHTSS) are widely used over highways across the nation. An overhead truss sign structure is comprised of a truss and two supporting frames at each end, and can be made using aluminum or steel. Aluminum overhead truss sign structures are generally more prone to vibration issues due to their light weight (Fouad, et al. 2003). Before 2015, aluminum overhead truss sign structures constructed in Kansas used an identical type of coupling assembly to provide connection between vertical poles and horizontal trusses. There are approximately 450 sign structures that use this type of connections over active highways in the State of Kansas. The coupler connection was designed in the early 1970s. At that time, experimental tests were conducted to determine the static strength of the connection (McCollom 1973), however, no prior research has been conducted to evaluate the fatigue performance of the coupler connection. Many of these connections have now been in service for 30-40 years and research is needed to evaluate the fatigue performance of the connections.

This report presents a study aimed at evaluating the fatigue performance of the coupler connections used in bridge-type overhead truss sign structures. It consists of two parts. The first part describes a series of finite element (FE) analyses that were used to determine the behavior of the coupler connections in expected real use. The results indicated that among all loading cases analyzed in this study, the out-of-plane responses of the sign structures were more significant than in-plane responses. The coupler connections behaved like idealized pinned connections, with little to no capability to transfer moments; therefore, the rivets connecting the interior two couplers were found to undergo mostly direct tension and shear. A rational experimental testing plan was developed according to the findings of the finite element analyses.

The second part of this study included performing 22 fatigue tests on newly-fabricated coupling assemblies obtained from Steve Johnson Fabrication, Inc. (Wichita, KS), the company that manufactures most OHTSS in Kansas. The experimental tests were conducted to characterize the fatigue performance of the coupler connection, utilizing AASHTO S-N curves. The fatigue tests were conducted in three directions, such that the rivet was loaded in: 1) tension, 2) vertical shear, and 3) horizontal shear. These loading conditions on the rivet represented, respectively: 1) truss out-of-plane shear, 2) truss in-plane shear, and 3) truss chord axial force. The testing program

revealed that the coupler connection has much better fatigue resistance when loaded in shear than in tension. Despite poor tensile fatigue performance, fatigue failure is still considered to be unlikely in OHTSS applications, due to very low stress demands found from finite element analyses.

Acknowledgements

The authors of this report would like to gratefully acknowledge the Kansas DOT for their support of this research, which was performed under KTRANS project KU-16-1.

Table of Contents

List of Figures	7
List of Tables	9
Introduction and Background.....	10
1.1 Background	10
1.2 Objective and Scope	13
Finite Element Analyses	14
2.1 Description of Models.....	14
2.2 Model Loading	17
2.3 Finite Element Analysis Results	19
2.3.1 – Connection Relative Rotation:	20
2.3.2 – Connection Moment:.....	23
2.3.3 – Deformation of Coupler Rivet:	24
2.3.4 – Location of Equivalent Point Load at Coupler Connection:.....	25
2.3.5 – In-Plane and Out-of-Plane Shear Forces at Connections:.....	26
2.3.6 – Load Reversal at Coupler Connections:	27
2.4 Conclusions from Finite Element Analyses	29
Description of Experimental Testing Program.....	30
3.1 Test Set-ups	30
3.2 Testing Plan.....	32
Experimental Program Results & Discussion	34
4.1 Rivet Loaded in Shear.....	34
4.2 Rivet Loaded in Tension	36
4.2.1 Specimens tested at 26.6 ksi:	37
4.2.2 Specimens tested at 15.1 ksi:	40
4.2.3 Specimens tested at 10.5 ksi:	41
4.2.4 Specimens tested at 8.3 ksi:	43
4.2.5 Specimens tested at 5.8 ksi:	45
4.2.6 Specimens tested at 4.2 ksi:	50
4.3 Discussion of Tension Test Results	50
4.4 Identifying Pre-Existing Cracks in Used Coupler	51
4.5 Confirmation of Coupler Material	53

4.6 Experimental Test Program Conclusions.....	53
Conclusions and Recommendations.....	55
References.....	56
APPENDIX A1 Loads Applied in FE Models.....	57
APPENDIX A2 Example Calculation of Fatigue Load.....	59
APPENDIX A3 Connection Rotations in FE Models	64
APPENDIX A4 Moment Diagrams of 60 ft Sign Structure	67

List of Figures

Figure 1. Bridge-Type Overhead Truss Sign Structure (OHTSS).....	10
Figure 2. Coupler Connection Used in Aluminum OHTSS in Kansas	12
Figure 3. Finite Element Models (with Detailed Connections) of OHTSS.....	15
Figure 4. Detailed Coupler Connection.....	16
Figure 5. Natural Wind and Truck-Induced Gust Load Placements.....	18
Figure 6. Truss Chord-to-Support Frame Connections.....	20
Figure 7. Connection Rotation Calculation in Detailed Model	21
Figure 8. Comparison of Detailed and Idealized Pinned Model Connection Relative Rotation for 60-ft OHTSS under NWB Loading	22
Figure 9. Minimum and Maximum Connection Relative Rotations.....	23
Figure 10. Moment Diagram of 60-ft OHTSS Chord 3-7 under Natural Wind Blowing from Back	24
Figure 11. Deformation of Rivet under 10x Increased Wind Loading (Magnification Scale 100x)	25
Figure 12. Location of Equivalent Point Load Over Cross-Section of Coupler Connection.....	26
Figure 13. Minimum and Maximum Section Force at Connections.....	27
Figure 14. Truss Displacement and Connection Shear under Gravity Load and Truck-Induced Gust	28
Figure 15. Comparison of Connection In-Plane Shear Induced by Gravity and Natural Wind....	29
Figure 16. Fatigue Test Setups for Coupler Connection.....	31
Figure 17. Schematic Drawings of Test Setups.....	31
Figure 18. Shear Test Setups Marked to Capture Sliding between Coupler and Pipe.....	32
Figure 19. S-N Curve – Coupler Connection Rivet Loaded in Horizontal Shear	35
Figure 20. S-N Curve – Coupler Connection Rivet Loaded in Vertical Shear	36
Figure 21. S-N Curve – Coupler Connection Rivet Loaded in Tension	37
Figure 22. Failure of FAT-TENS(USED)1 Tested at 26.6 ksi.....	38
Figure 23. Failure Surface of FAT-TENS(USED)1	38
Figure 24. Failure of FAT-TENS(USED)2 Tested at 26.6 ksi.....	39
Figure 25. Failure of FAT-TENS1 Tested at 26.6 ksi.....	39
Figure 26. Failure of FAT-TENS13 Test at 15.1 ksi	40

Figure 27. Stiffness vs. Number of Cycles for FAT-TENS13 Tested at 15.1 ksi	40
Figure 28. Failure of FAT-TENS11 Tested at 10.5 ksi.....	41
Figure 29. Stiffness vs. Number of Cycles for FAT-TENS11 Tested at 10.5 ksi	41
Figure 30. Failure of FAT-TENS12 Tested at 10.5 ksi.....	42
Figure 31. Stiffness vs. Number of Cycles for FAT-TENS12 Tested at 10.5 ksi	42
Figure 32. Failure of FAT-TENS2 Tested at 8.3 ksi	43
Figure 33. Failure of FAT-TENS3 Tested at 8.3 ksi	44
Figure 34. Stiffness vs. Number of cycles for FAT-TENS3 Tested at 8.3 ksi	44
Figure 35. Failure of FAT-TENS9 Tested at 8.3 ksi	45
Figure 36. Stiffness vs. Number of Cycles for FAT-TENS9 Tested at 8.3 ksi	45
Figure 37. Cracking of FAT-TENS4 Tested at 5.8 ksi	46
Figure 38. Failure of FAT-TENS4 Tested at 5.8 ksi	46
Figure 39. Stiffness vs. Number of Applied Cycles for FAT-TENS5 Tested at 5.8 ksi.....	47
Figure 40. Failure of FAT-TENS5 Tested at 5.8 ksi	47
Figure 41. Stiffness vs. Number of Cycles for FAT-TENS5 Tested at 5.8 ksi	48
Figure 42. Failure of FAT-TENS7 Tested at 5.8 ksi	48
Figure 43. Stiffness vs. Number of Cycles for FAT-TENS7 Tested at 5.8 ksi	49
Figure 44. Failure of FAT-TENS8 Tested at 5.8 ksi	49
Figure 45. Stiffness vs. Number of Cycles for FAT-TENS8 Tested at 5.8 ksi	49
Figure 46. Failure Surface of Microscopic Photograph of FAT-TENS(USED)1	52
Figure 47. Corrosion Products on Failure Surface of FAT-TENS4	52
Figure 48. Photomicrograph of Coupler Material Sample	53

List of Tables

Table 1. Finite Element Model Material Properties.....	16
Table 2. Finite Element Model Contact and Interaction Properties.....	17
Table 3. Ratio of Torque and Shear at End of Truss Chord of 60-ft OHTSS	25
Table 4. Fatigue Testing Matrix	33

Introduction and Background

1.1 Background

Bridge-type overhead truss sign structures (OHTSS) are widely used on highways across the United States. As shown in Figure 1, these structures are comprised of a horizontal 3D space truss and a support frame at each end. OHTSS can be made of either steel or aluminum; Kansas OHTSS are nearly exclusively aluminum. Many commonly-used connections details for OHTSS and other sign structures can be found in Chapter 11 of the AASHTO Specifications for Structural Supports for Highway Signs, Luminaires, and Traffic Signals (AASHTO 2009). However, many state DOTs use specialized connections that are not documented in the specifications.



Figure 1. Bridge-Type Overhead Truss Sign Structure (OHTSS)

Compared to cantilevered sign structures, non-cantilevered sign structures are usually considered to be less sensitive to fatigue damage. Kacin, et al. (2010) presented the results of a study focused on predicting the fatigue life of OHTSS; they gathered wind data, created dynamic finite element models, and inputted wind action simulated using mathematical models. The results indicated that the evaluated connections were all within the infinite fatigue limit range. However, some other studies, such as one performed by Mclean, et al. (2004) in which two overhead truss sign structures were evaluated using both finite element analyses and field testing, have indicated that stresses in some members could exceed the constant amplitude fatigue limit.

Overhead truss sign structures are not immune to fatigue damage. A report to the Illinois DOT presented photographs of several failures at web diagonal strut-to-chord connections in aluminum overhead sign structures (Foutch, et al. 2006). Foley, et al. (2004) discussed the failure

of a bridge-type overhead sign structure and indicated that the cracking was initiated by liquid metal embrittlement during the galvanizing process. A survey conducted as part of NCHRP Project 17-10(2) indicated that eight out of 25 responding state DOTs reported fatigue-related problems associated with overhead truss sign structures (Fouad, et al. 2003). Moreover, although it is recognized that steel OHTSS rarely have vibration problems because of their weight, aluminum structures can be more sensitive to this due to their lightness (Fouad, et al. 2003), which can accelerate fatigue damage.

The wind loads that need to be considered in fatigue design of OHTSS include galloping, natural wind, vortex shedding, and truck-induced gusts (AASHTO 2009). For non-cantilevered structures, galloping and vortex shedding are generally not considered significant concerns. The AASHTO Specifications for Structural Supports for Highway Signs, Luminaires, and Traffic Signals (AASHTO 2009) only specify that natural wind and truck-induced gusts should be considered in the design of non-cantilevered structures. In the existing literature, the structural response induced by truck-induced gusts is recognized to usually be less than that induced by natural wind (Dexter and Ricker 2002). In addition, Dexter and Ricker (2002) indicated that the design pressures used for truck-induced gust loading may be significantly overestimated. AASHTO (2009) indicates that truck-induced gust loading should not be considered for OHTSS unless required by the owner.

Many studies have been conducted to determine the fatigue properties of the connections used in sign structures. Mirza, et al. (1975) presented an early study conducted on two tri-chord OHTSS. Fatigue testing was conducted on the flange connection of a chord-splice. No sign of fatigue damage was observed after 1 million cycles. Kaczinski, et al. (1998) presented tests conducted on cantilevered overhead sign structures (COSS). Based on a review of previous research at the time, it summarized connections into five categories, including: plain members, mechanically-fastened connections, groove-welded connections, fillet-welded connections, and attachments (Kaczinski, et al. 1998). Among these, mechanically-fastened connections (including bolted connections, anchor bolt details, mechanical clamps, and U-bolts) were classified as AASHTO Category D fatigue details. Welded connections were mostly categorized as Category E or E' (Kaczinski, et al. 1998). Appendix C of NCHRP Report 494 (Fouad, et al. 2003), which

specifically discussed fatigue design of non-cantilevered sign structures, adopted the same classification. It summarized 13 example details that were commonly used in non-cantilevered sign structures. Among these details, Example 3 was a typical beam-column connection. The connection consisted of a bolted coupler detail used to attach to the vertical pole and a welded detail to connect the beam. The welded detail was Category E'. The bolted coupler detail that attached to the pole was similar to the connection evaluated in this study, and was classified as Category D.

Nearly all aluminum OHTSS constructed in Kansas before 2015 use an identical type of coupling assembly to connect the vertical poles and horizontal trusses. There are approximately 450 sign structures that use this type of connection over Kansas highways. As shown in Figure 2, each connection assembly consists of four half-couplers. The interior two half-couplers are riveted together in a fabricating shop. During construction, the exterior half-couplers are bolted onto the riveted interior pieces to hold the pole and the truss chord in place. The couplers are made of ductile cast iron, as determined through external testing conducted during this project. Threaded steel rod segments are glued onto the inside of the couplers using silicone. The threaded rod segments, known as “keepers,” function as gripping devices to prevent the pipes from sliding in the connection.



(a) Coupling Assembly



(b) Interior of Coupler

Figure 2. Coupler Connection Used in Aluminum OHTSS in Kansas

In addition to the self-weight of the structure, the primary loads resisted by OHTSS are wind loads, including natural wind gusts and truck-induced gusts (AASHTO 2009). Given that wind loads are periodic, the fatigue behavior of the coupler connections is essential to understand.

The coupler connection was originally designed in the early 1970s. At that time, experimental tests were conducted to determine the static strength of the connection (McCullom 1973). However, no research has been conducted to evaluate the fatigue performance of the coupler connection used in KDOT's inventory of OHTSS. In the meantime, the average age of Kansas' inventory of OHTSS has continued increasing; many of the connections have been in service for 30-40 years. Research is needed to evaluate the fatigue strength of the connections.

1.2 Objective and Scope

This study was aimed at characterizing the fatigue performance of coupler connections used in Kansas OHTSS, and consisted of two parts. The first was a series of finite element (FE) analyses, conducted using the commercially-available finite element analysis software Abaqus v.2016. The FE analyses were used to determine global behavior of the sign structures and expected structural demands on the coupler connections in use. Sign structures with four different spans were modeled. Six loading modes and three truss chord-to-supporting frame connection properties were considered. Using the results from these FE analyses, realistic load ranges for in-service structures were determined, and rational experimental testing setups were developed.

The second part of the study included 22 fatigue tests of coupler connections, conducted on coupling assemblies obtained from Steve Johnson Fabrication, Inc., which is the company that manufactures most overhead truss sign structures in Kansas. The 22 fatigue tests were divided into three groups, with respect to the direction of the stress in the rivet connecting the two interior half-couplers: (1) tension, (2) horizontal shear, and (3) vertical shear.

In addition to the 22 tests conducted using newly-fabricated coupler assemblies, two coupler assemblies taken from an OHTSS that was removed from service were also tested. After fatigue testing, the failure surfaces of these couplers were microscopically examined to evaluate the possibility of pre-existing cracks.

Material samples were extracted from a coupler and were analyzed by Pacific Testing Laboratories, INC. (Valencia, CA) to determine the couplers' material composition.

Finite Element Analyses

Four sign structures with spans of 60 ft, 83 ft, 110 ft, and 137 ft were modeled based on drawings and input provided by the Kansas DOT. The four OHTSS chosen for analysis all had truss chords with a nominal diameter of 8 in. (8-5/8 in. actual diameter) and supporting frame pipes with a nominal diameter of 10 in. (10-3/4 in. actual diameter). The structural responses were determined by applying fatigue loads calculated using the AASHTO Specifications for Structural Supports for Highway Signs, Luminaires, and Traffic Signals (AASHTO 2009). Six loading modes were applied within each model, including natural wind applied at the front, back, and side of the OHTSS, and truck-induced gusts applied at the right, middle, and left of the structure. Three types of boundary conditions were investigated for the connections between the truss chord and vertical supporting frame, including: idealized pinned connections, idealized rigid connections (tied), and inclusion of detailed 3D connection models.

2.1 Description of Models

Four OHTSS with spans of 60 ft, 83 ft, 110 ft, and 137 ft were modeled using the commercially-available software package Abaqus. For the models shown in Figure 3, the main bodies of the structures were simulated using 2-node linear 3D beam elements (B31), while the connections were created using 8-node linear brick 3D solid elements (C3D8R) to resemble the geometries of the coupling assemblies as close as possible. These particular models are referred as ‘detailed models’ throughout this report.

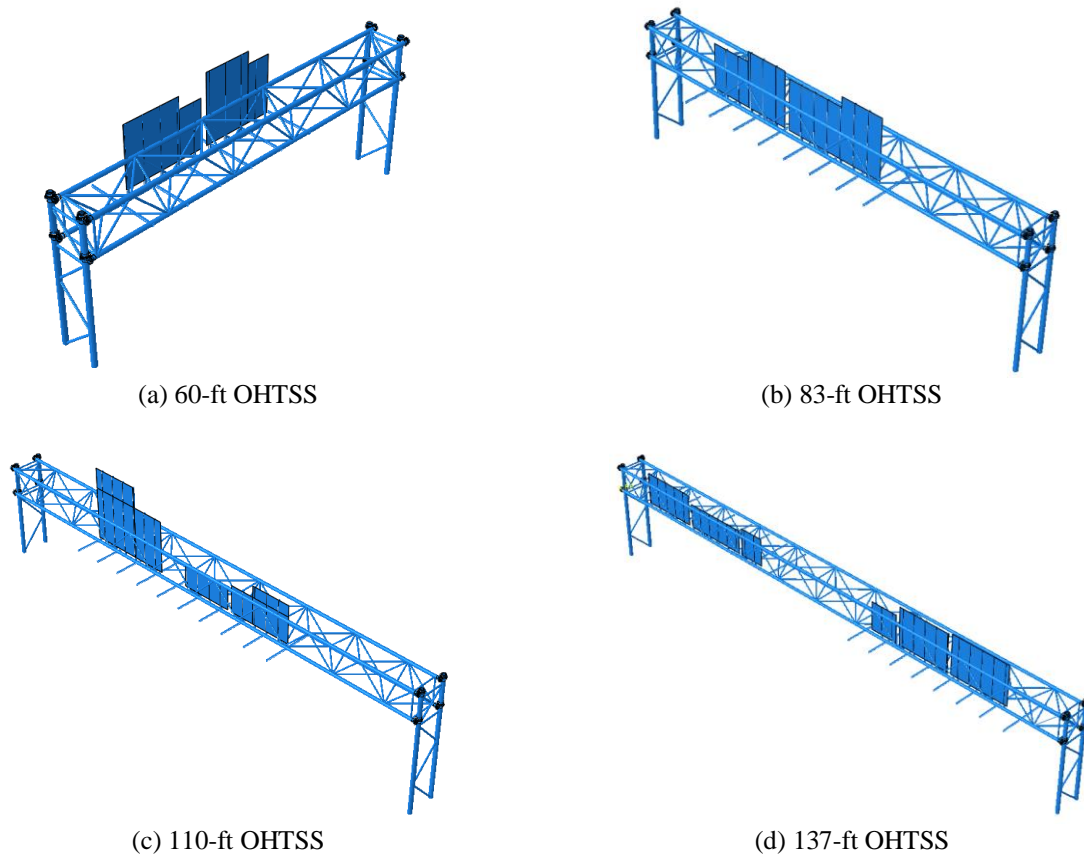


Figure 3. Finite Element Models (with Detailed Connections) of OHTSS

A closer look of the detailed coupler connection is shown in Figure 4. In addition to the detailed models that included explicitly-modeled couplers, models were also created that included simple pinned and tied (rigid) connections between the truss chord and support frame. In these models, the coupler connections were not explicitly simulated, and the connections were idealized as either a pin or a tie. In the models with pinned connections between the chord and support frame, the three translation degrees of freedom of the two nodes at the joint of chord and support frame were restrained. In the tied connection models, all six degrees of freedom were restrained, mimicking the behavior of a moment-type connection.

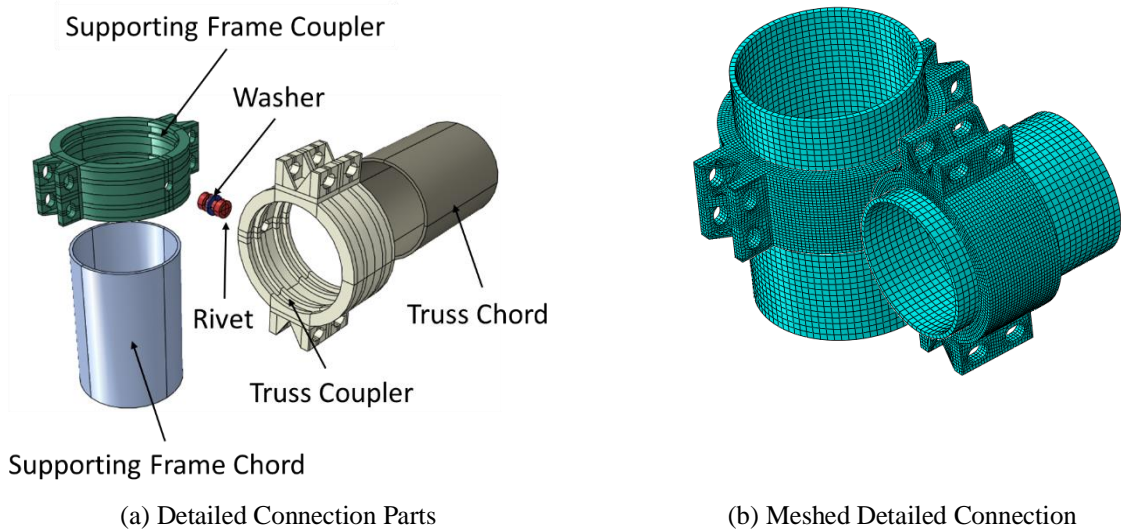


Figure 4. Detailed Coupler Connection

Table 1 lists the material properties for aluminum, steel, and ductile cast iron adopted in the models of this study. All materials were modeled as linear-elastic.

Table 1. Finite Element Model Material Properties

	Parts	Density (kip/in³)	Modulus of Elasticity (ksi)	Poisson's Ratio
Aluminum	Sign, Truss, Sign Beam, Walkway Beam, Supporting Frame	0.098	10000	0.35
Steel	Rivet, Washer	0.284	29000	0.3
Ductile Cast Iron	Coupler	0.284	24000	0.275

The contact and interaction properties used in the models are presented in Table 2. A *tie constraint* indicates that all degrees of freedoms for two nodes in a contact pair are restrained to each other. *Hard contact* minimizes the penetration between two contact surfaces and does not transfer tensile stress across the contact interface. A friction coefficient of 0.5 was defined in models for which hard contact properties were specified. Kinematic coupling restrained the nodes on solid element truss chord cross-section to the rigid body movement of the node of the beam element truss chord.

Table 2. Finite Element Model Contact and Interaction Properties

Contact Pair	Contact Property
Coupler – Truss Chord (Solid Elements)	Tie
Coupler – Rivet Head	Tie
Coupler – Rivet Shank	Hard Contact
Washer – Rivet Shank	Hard Contact
Washer - Coupler	Hard Contact
Sign-Sign Beam	Tie
Sign Beam - Truss Chord (Beam Elements)	Pin
Walkway Beam - Truss Chord (Beam Elements)	Pin
Truss Chord (Solid Elements) - Truss Chord (Beam Elements)	Kinematic Coupling (All DOFs)

2.2 Model Loading

Fatigue loads for highway sign structures (AASHTO 2009) were applied in the models, calculated using (Equation 1 and (Equation 2. The study considered six loading modes, including natural wind load applied at the front, back, and side of the structures, and truck-induced gusts applied at the right, middle, and left of the structures.

Natural Wind Gust:

$$P_{NW} = 5.2C_d I_F \quad \text{(Equation 1)}$$

Truck Induced Gust:

$$P_{TG} = 18.8C_d I_F \quad \text{(Equation 2)}$$

Where,

C_d = Drag Coefficient

I_F = Fatigue Importance Factor

According to AASHTO (2009), natural wind gust loading is to be applied in the horizontal direction to the exposed area of all members, and truck-induced gust loading is to be applied in the vertical direction along any 12 ft length excluding any portion not located directly above a traffic line. In this study, the natural wind gust loading was applied to the back, front, and side of the sign

structures, and the truck-induced gust was applied over a 12-ft length at the right, left, and middle of the trusses. The load placements applied in the model of the 60-ft sign structure are presented in Figure 5 as an example. All loads were applied as static loads in Abaqus.

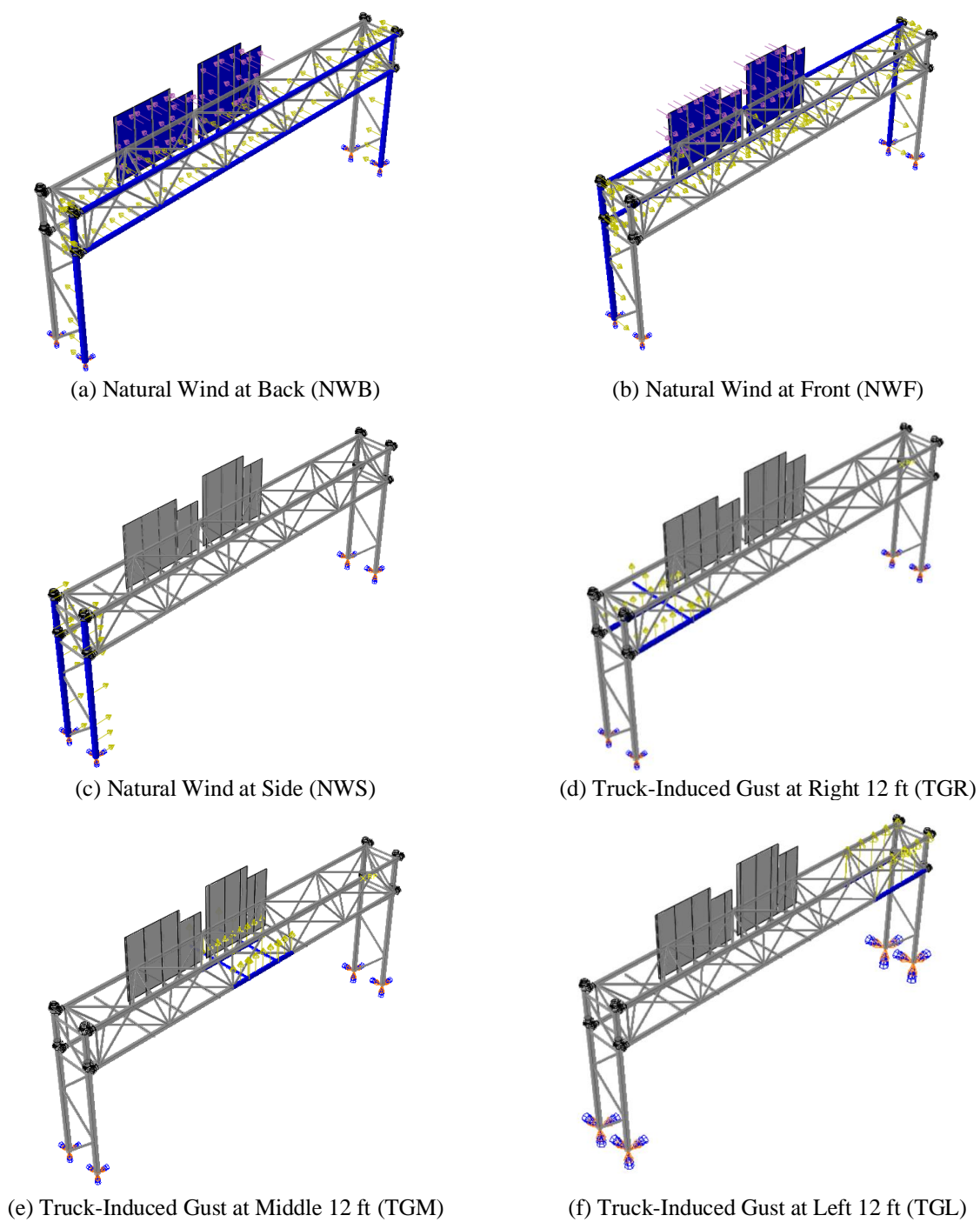


Figure 5. Natural Wind and Truck-Induced Gust Load Placements

The loads acting on the web diagonal struts of truss panels and supporting frames were calculated and distributed onto the truss chords and the supporting frame columns. All loads applied in each model are summarized in Appendix A1. Additionally, Appendix A2 presents an example calculation for the 60-ft span OHTSS.

In addition to the design loads applied to the OHTSS, an initial pretension force was also applied to the rivet in the models that included explicit modeling of the coupler connection. The initial tension in each rivet was taken as approximately equal to its material yield strength (Munse 1956). Since the yield strength of a high strength rivet is about 38 ksi, a 38 ksi pretension stress was adopted in a separate step before wind loads were applied.

2.3 Finite Element Analysis Results

This section presents and discusses results obtained from the finite element analyses. These results provided valuable insights in choosing rational test setups and load ranges for experimental testing. For easier presentation, each truss chord to supporting-frame connection is labeled and shown in Figure 6. This report uses the following terms to describe the direction of moment and shear:

1. In-plane: the plane parallel to the plane of the truss, which is the Y-Z plane shown in Figure 6;
2. Out-of-plane: the plane perpendicular to the plane of the truss, which is the X-Z plane.

Following this convention, in-plane shear refers to shear in the Y-direction; in-plane moment refers to moment occurring about the X-axis; out-of-plane shear refers to shear in X-direction; and out-of-plane moment refers to moment about the Y-axis.

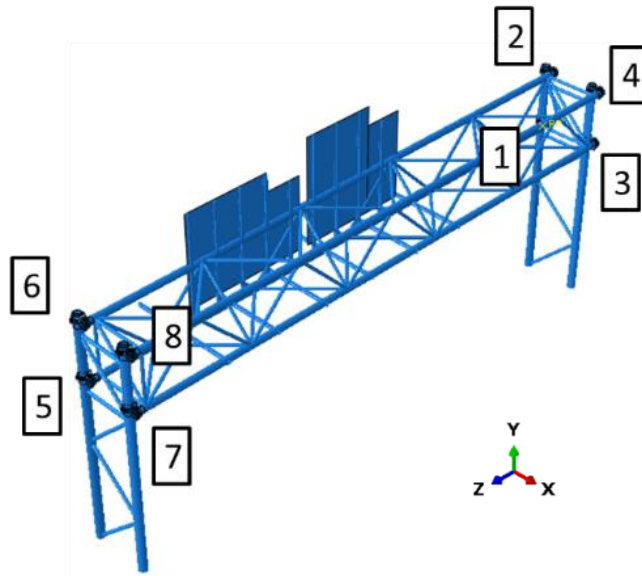


Figure 6. Truss Chord-to-Support Frame Connections

As introduced previously, six loading modes were considered in the analyses. Only natural wind blowing from the back of sign (NWB) and truck-induced gusts applied over the middle 12 ft (TGM) and right 12 ft (TGR) are reported here due to the following reasons:

1. Natural wind blowing from the front of sign (NWF) resulted in a similar response as found for wind blowing from the back. The responses observed for the NWF loading case were usually lower magnitude than for the NWB loading direction, since the segments of truss chord behind the sign were not loaded in the NWF case.
2. Natural wind blowing from the side of structure (NWS) produced a lesser response than other loading modes.
3. The differences between the responses of truck-induced gust applied at left 12 ft (TGL) and right 12 ft (TGR) were found to be negligible.

2.3.1 – Connection Relative Rotation:

The relative rotation of the coupler connection in the detailed model was obtained by calculating the deformed angle of two lines parallel to each other on the edge of the truss chord coupler and the supporting-frame coupler.

As shown in Figure 7, the rotation in the Y-Z plane, which is the rotation in the plane of the truss, can be obtained by calculating the deformed angle of either lines 1 and 3 or lines 2 and 4. The rotation in the X-Z plane, which is the rotation out of the plane of truss, can be obtained by comparing lines 1 and 3. Similarly, the rotation in X-Y plane can be obtained by comparing lines 2 and 4. Relative rotations in pinned connections were obtained by calculating the difference between absolute rotations of nodes on truss chords and supporting frames at their junctions. In the tied connection models, which represent fully-restrained end connections, the relative rotations were always zero, since all the degree of freedoms of the nodes at the joints of truss chords and supporting frames were restrained (rigid connection rotation).

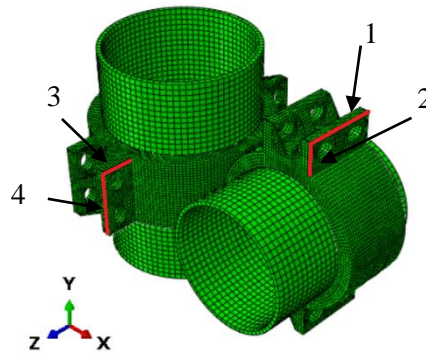
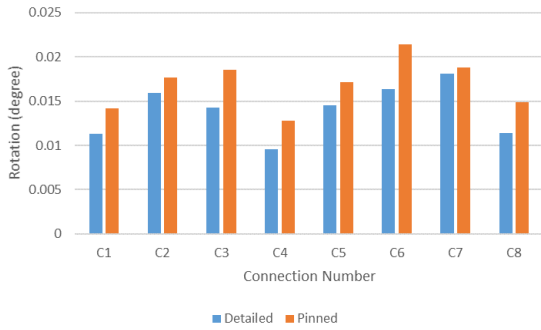
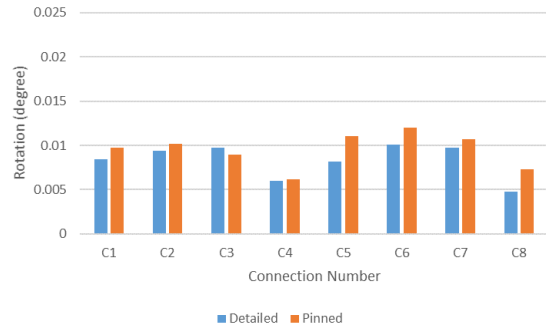


Figure 7. Connection Rotation Calculation in Detailed Model

A comparison between the detailed and idealized pinned models for the 60-ft span sign structure under the loading mode of natural wind blowing from back of the sign panel (NWB) is presented in Figure 8. The computed connection relative rotations for all span lengths and various loading modes included in the study are presented in Appendix A3. It was found that the detailed connection models reached at least 70% of the rotations computed for the idealized pinned connections.



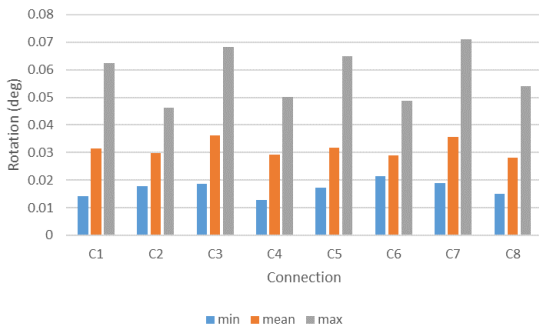
(a) Out-of-Plane Rotation



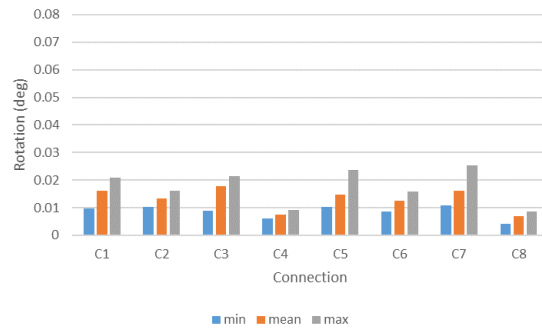
(b) In-Plane Rotation

Figure 8. Comparison of Detailed and Idealized Pinned Model Connection Relative Rotation for 60-ft OHTSS under NWB Loading

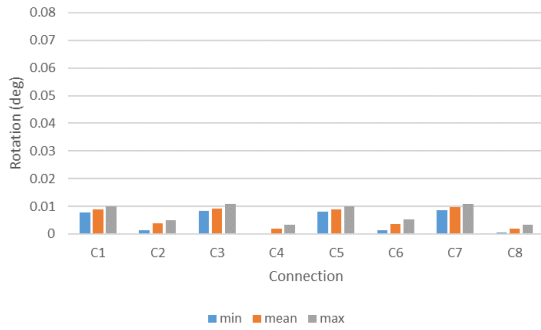
Figure 9 presents the minimum, average, and maximum values of the relative rotations for the connections from the 60-ft, 83-ft, 110-ft, and 137-ft OHTSS. Although natural wind acts in the out-of-plane direction, it was found to induce both out-of-plane and in-plane rotations, as shown in Figure 9(a) and Figure 9(b). The out-of-plane response was larger, but the in-plane response was non-negligible. Truck-induced gust loading, however, only induced rotations in the in-plane direction. In general, the response in the in-plane direction was much smaller than those observed in the out-of-plane direction.



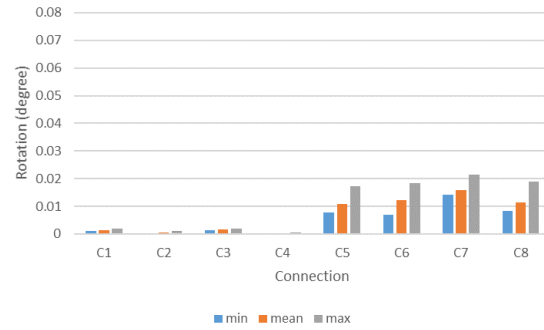
(a) Out-of-Plane Rotation under Natural Wind from Back (NWB) of Structure



(b) In-Plane Rotation under Natural Wind from Back (NWB) of Structure



(c) In-Plane Rotation under Truck-Induced Gust at Mid 12 ft



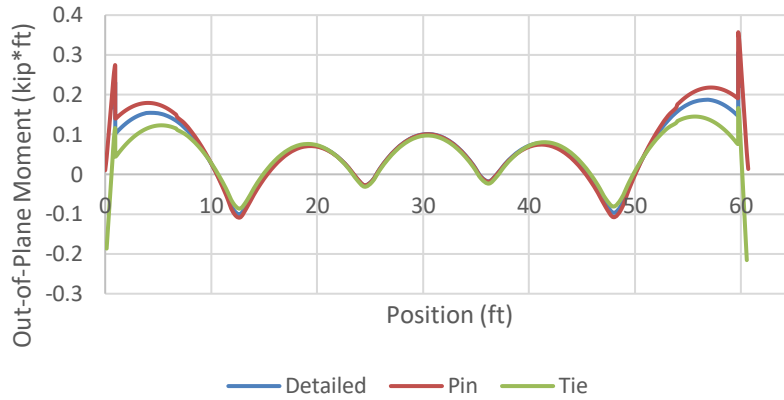
(d) In-Plane Rotation under Truck-Induced Gust at Right 12 ft

Figure 9. Minimum and Maximum Connection Relative Rotations

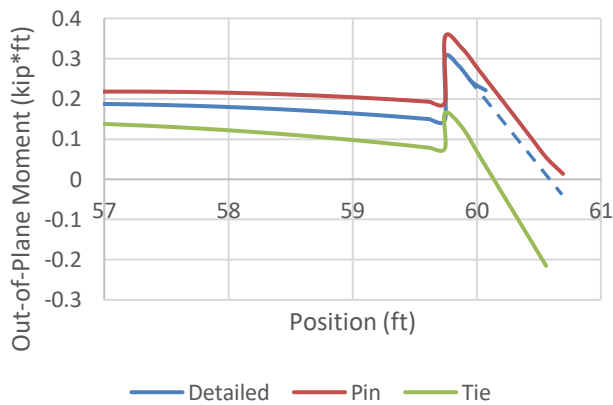
2.3.2 – Connection Moment:

The moment diagram for Chord 3-7 in the 60-ft OHTSS under natural wind blowing from the back (NWB) of the structure is shown in Figure 10(a). This diagram provides a comparison of the structural response for the three different connection modeling techniques (idealized pinned, idealized fully-restrained, and detailed model). The moment diagram for the first four feet (connection 3 side) is shown in Figure 10(b). There is an instantaneous spike in moment at a distance approximately 1 ft away from the connection, because web diagonal struts meet the chord at that location, as illustrated in Figure 10(c). Additional moment diagrams for the 60-ft OHTSS can be found in Appendix A4.

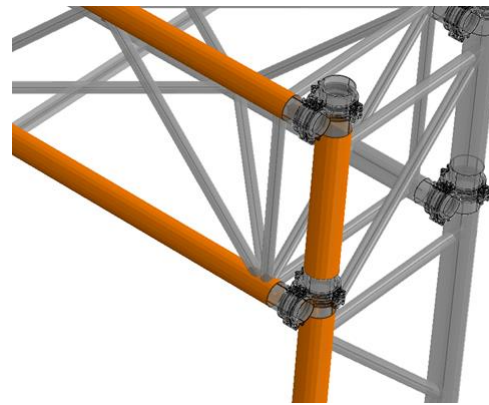
As shown by the solid blue line in Figure 10(b), which represents the detailed connection model, moment data is not available for the first 0.7 ft of the connection since the connection was modeled using solid elements. However, the moment at a connection can be predicted by following the same slope of the solid blue line since the shear force is constant between a connection and a joint of web diagonal struts, as shown by the dashed blue line in Figure 10(b). The moment predicted by the dashed blue line is only about 10% of the moment in the tied connection model. This indicates the behavior of the coupler connection is more similar to that of an idealized pinned connection than an idealized fully-restrained connection.



(a) Moment Diagram of Chord 3-7 of 60-ft OHTSS



(b) Moment Diagram at Connection 7



(c) Web Diagonal Struts at Connection 7

Figure 10. Moment Diagram of 60-ft OHTSS Chord 3-7 under Natural Wind Blowing from Back

2.3.3 – Deformation of Coupler Rivet:

The rivet response in the coupler connection was considered under wind loading, to help develop an understanding of dominant load components acting on it. However, deformation of the coupler rivets under wind loads could not be visualized in the original models, because the fatigue loads were too small relative to the pretension forces applied to the rivets. Therefore, to examine rivet deformation caused by wind loads, the natural wind gust load in the 60 ft span structure model was increased by 10 times. The resulting deformation mode of a rivet under this loading is shown in Figure 11, magnified 100x. The rivet showed negligible deformations in bending or twisting.

Therefore, this finding revealed that tension and shear are the dominant load components on the coupler connection rivets.

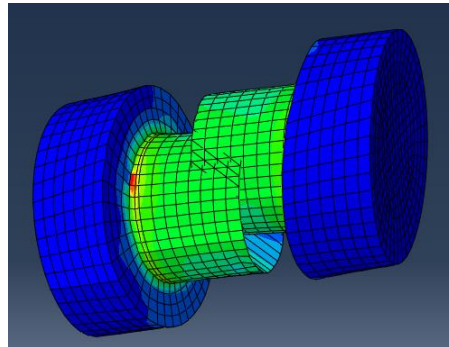


Figure 11. Deformation of Rivet under 10x Increased Wind Loading (Magnification Scale 100x)

2.3.4 – Location of Equivalent Point Load at Coupler Connection:

As a further means to consider the types of forces that the rivet is subjected to, the ratios of torque and shear at the ends of the truss chords of the 60 ft span sign structure were calculated (Table 3).

Table 3. Ratio of Torque and Shear at End of Truss Chord of 60-ft OHTSS

Connection Number	Natural Wind (Back) (in.)	Truck Gust (Middle) (in.)	Truck Gust (Right) (in.)
1	4.8	4.7	4.6
2	4.6	5.2	5.5
3	4.7	4.8	4.7
4	5.2	5.0	5.1
5	4.7	4.7	4.5
6	4.4	5.2	5.1
7	4.7	4.8	4.6
8	5.1	5.0	4.9

The ratios indicate the distance between the center of the chord and the location of the equivalent point load over the cross-section of the coupler connection. The ratios are all close to 5 in. It is worth noticing that the distance between the chord center and the rivet center is 5.28 in. in the model. This indicates the equivalent point load is located close to the center of rivet over the cross-section of the coupler connection, as shown in Figure 12. The result is as predicted since the stiffness of the truss is large. A twisting motion that causes rivets to bend is less likely to occur.

This finding shows that care should be taken to not to cause bending in the rivets when designing the fatigue test setup.

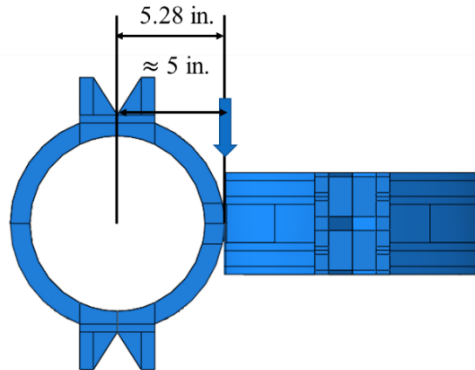


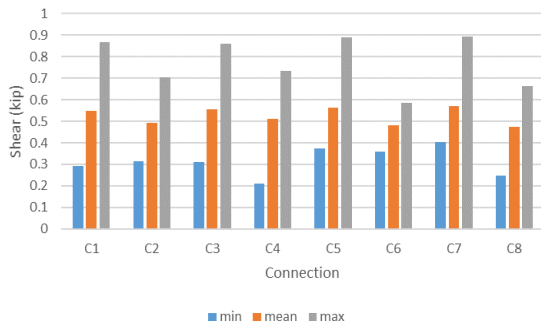
Figure 12. Location of Equivalent Point Load Over Cross-Section of Coupler Connection

2.3.5 – In-Plane and Out-of-Plane Shear Forces at Connections:

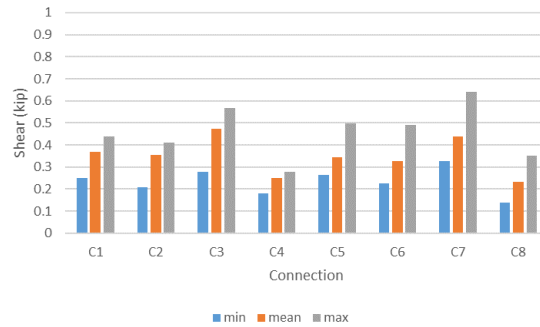
As discussed, the coupler connection behavior was found to be more similar to a pinned connection than to a fully-restrained (tied) connection. The moments at the coupler connections were found to be small, and shear and axial forces were the primary load components at the truss ends.

The minimum, average, and maximum section forces at connections obtained from the 60-ft, 83-ft, 110-ft, and 137-ft models are presented in Figure 13. The horizontally-applied natural wind load induced both in-plane and out-of-plane shear effects, with out-of-plane shear more dominant in general. The in-plane shear induced by natural wind can be 20%-110% of the out-of-plane shear at the same connection, with an average of about 70%. Truck-induced gust loading, however, was found to only induce shear in the in-plane direction. The maximum axial force at coupler connections induced by natural wind ranged from 3-70% of the out-of-plane shear, with an average of 20%. For truck-induced gust loading applied at the middle span, the axial force ranged from 20%-240% of the in-plane shear at the same coupler connection, with an average of 80%. The axial forces induced by truck-induced gust at the side of the span were found to be negligible. Among all span lengths and loading modes, the maximum out-of-plane shear force for all span lengths and load cases was found to be less than 1 kip. The maximum in-plane shear was approximately 0.7 kip. The maximum axial force was approximately 0.5 kip. For all the OHTSS

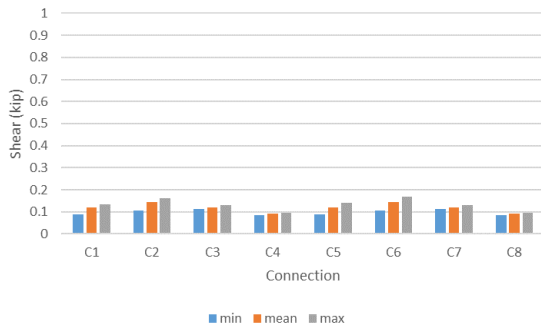
included in the study, the response produced by natural wind was always more significant than the response to truck-induced gust loading.



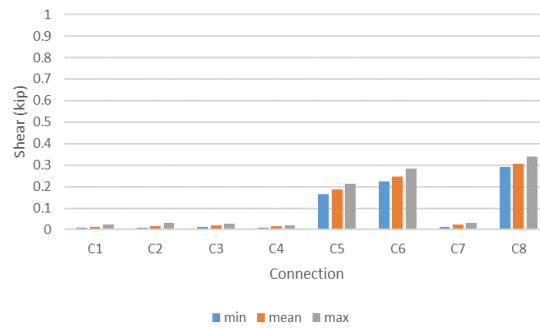
(a) Out-of-Plane Shear under Natural Wind from Back



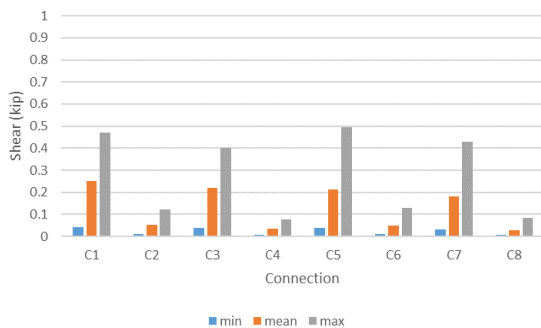
(b) In-Plane Shear under Natural Wind from Back



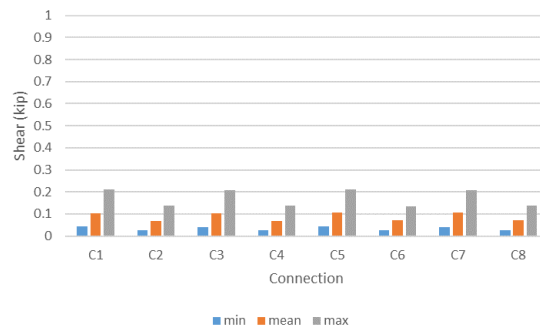
(c) In-Plane Shear under Truck-Induced Gust at Middle



(d) In-Plane Shear under Truck-Induced Gust at Right



(e) Axial Force under Natural Wind from Back



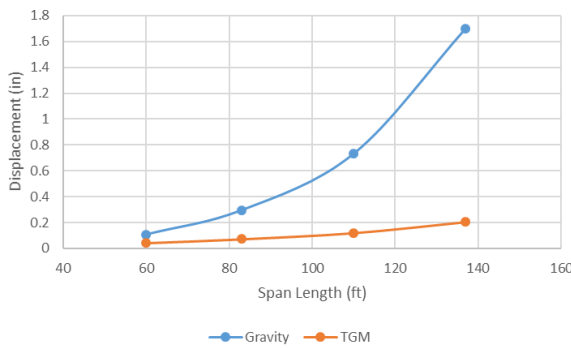
(f) Axial Force under Truck-Induced Gust at Middle

Figure 13. Minimum and Maximum Section Force at Connections

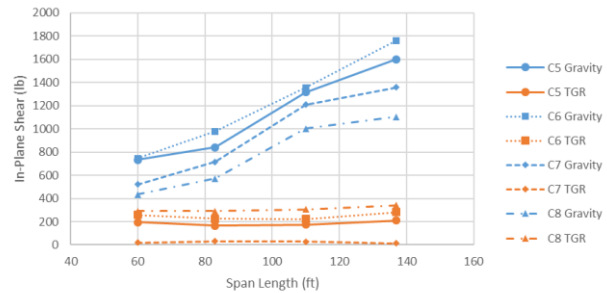
2.3.6 – Load Reversal at Coupler Connections:

When considering out-of-plane response, only the direction that causes the rivet to be in tension needs attention. Forces in the other direction are transferred through bearing of the two

couplers, and therefore do not contribute to fatigue cracking. It is conservative to not consider load reversal in the out-of-plane direction. However, load reversal would need to be considered if the response in the in-plane direction were to overcome gravity loads. A comparison of the displacement and connection shear under truck-induced gust is presented in Figure 14, showing that displacements and shears induced by truck-induced gust loading are all smaller than those induced by the self-weight of the structure. This indicates load and displacement reversal is not expected to occur under truck-induced gust loading.



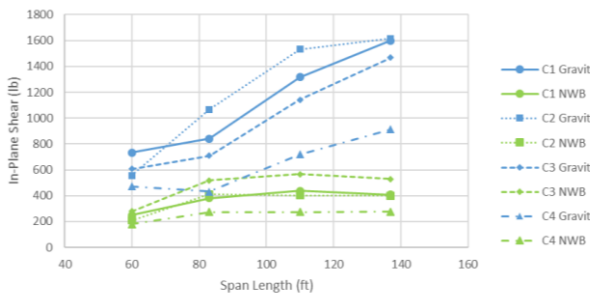
(a) Displacement at Center of Truss under Gravity Load and Truck-Induced Gust at Mid-12 ft



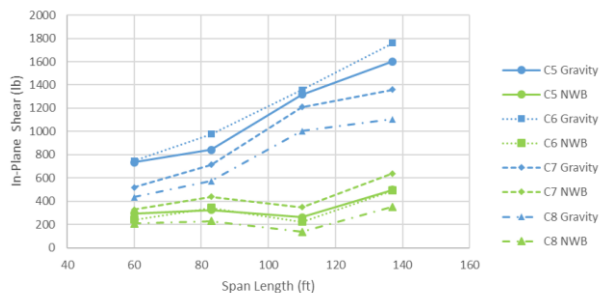
(b) In-Plane Shear at Connections 5, 6, 7, 8 under Gravity Load and Truck-Induced Gust at Right 12 ft

Figure 14. Truss Displacement and Connection Shear under Gravity Load and Truck-Induced Gust

As discussed, the horizontally-applied natural wind load was found to induce both out-of-plane and in-plane shear at the coupler connection. Figure 15 presents the in-plane shear in a coupler connection under gravity and natural wind gust loading. None of the in-plane shear induced by the natural wind at a connection was found to exceed its corresponding shear due to gravity, indicating that load reversal does not occur.



(a) In-Plane Shear at Connections 1, 2, 3, 4 under Gravity Load and Natural Wind Gust



(b) In-Plane Shear at Connections 5, 6, 7, 8 under Gravity Load and Natural Wind Gust

Figure 15. Comparison of Connection In-Plane Shear Induced by Gravity and Natural Wind

2.4 Conclusions from Finite Element Analyses

The series of finite element analyses conducted in this study were aimed at understanding the behavior of coupler connections in expected real use and were necessary to provide information for designing a rational experimental test setup. The following conclusions were reached:

- Analyses of connection rotations and moments indicated that the behavior of the coupler connection in OHTSS is more like a pinned connection than to a fully-restrained connection. Moments at the coupler connections under AASHTO (2009) design fatigue loading were found to be negligible.
- Rivets in coupler connections were found to experience negligible twisting and bending deformations, indicating that the rivets are subjected to direct tension and shear in service. Therefore, the physical testing program should focus on fatigue tests that produce tension and shear in the coupler rivet.
- The response of OHTSS under natural wind load was more significant than that under truck-induced gusts.
- Across all fatigue load cases and span lengths included in this study, the maximum out-of-plane shear (produces tension in the rivet), in-plane shear (produces shear in the rivet), and axial load (produces shear in the rivet) were found to be approximately 1 kip, 0.7 kip, and 0.5 kip, respectively (1.7 ksi, 1.2 ksi, and 0.8 ksi with respect to the rivet cross-sectional area). Other load components were found to be negligible.
- The fatigue responses at the rivet were not found to overcome the effects of gravity load, therefore, load reversal effects do not need to be considered in the experimental testing program.

Description of Experimental Testing Program

Based on the findings from the finite element analyses that considered a range of OHTSS with different span lengths subjected to natural wind loading and truck-induced gust loading, in-service coupler connections were found to be primarily loaded in direct shear and tension. Therefore, to evaluate the fatigue performance of the riveted coupler connection, this study included a series of physical tests conducted in three loading modes: 1) rivet loaded in tension; 2) rivet loaded in vertical shear; 3) rivet loaded in horizontal shear.

Out-of-plane shear forces in the OHTSS induce tension in the coupler rivets, and in-plane shear forces in OHTSS induce vertical shear in the coupler rivets. Axial loads applied through the truss chords at connections induce horizontal shear in the coupler rivets. Although the finite element analyses indicated that axial loads at truss chord ends were negligible under the action of design fatigue loads, specimens were still tested with rivets loaded in horizontal shear for completeness of the study and to fully characterize the fatigue performance of the connection under different loading directions.

3.1 Test Set-ups

As shown in Figure 16, three different test setups were designed to test coupler connections under the loading modes that produced vertical shear, horizontal shear, and tension in the coupler rivet.



(a) Vertical Shear



(b) Horizontal Shear



(c) Tension

Figure 16. Fatigue Test Setups for Coupler Connection

In the shear test setups, the couplers were used to connect a horizontal and a vertical pipe, with the horizontal pipe supported at its ends and the vertical pipe connected to an actuator. In the test setup used to apply horizontal shear on the rivet, the support frame pipe (10 in. pipe) was in the horizontal position, as shown in Figure 17(a). For the vertical shear test setup, the positions of the 10-in. and 8-in. pipes and couplers were reversed. A closed-loop servo-controlled MTS actuator was used to apply cyclical (sinusoidal) fatigue loads, and was carefully placed such that the load was aligned with the center of the rivet to create direct shear.

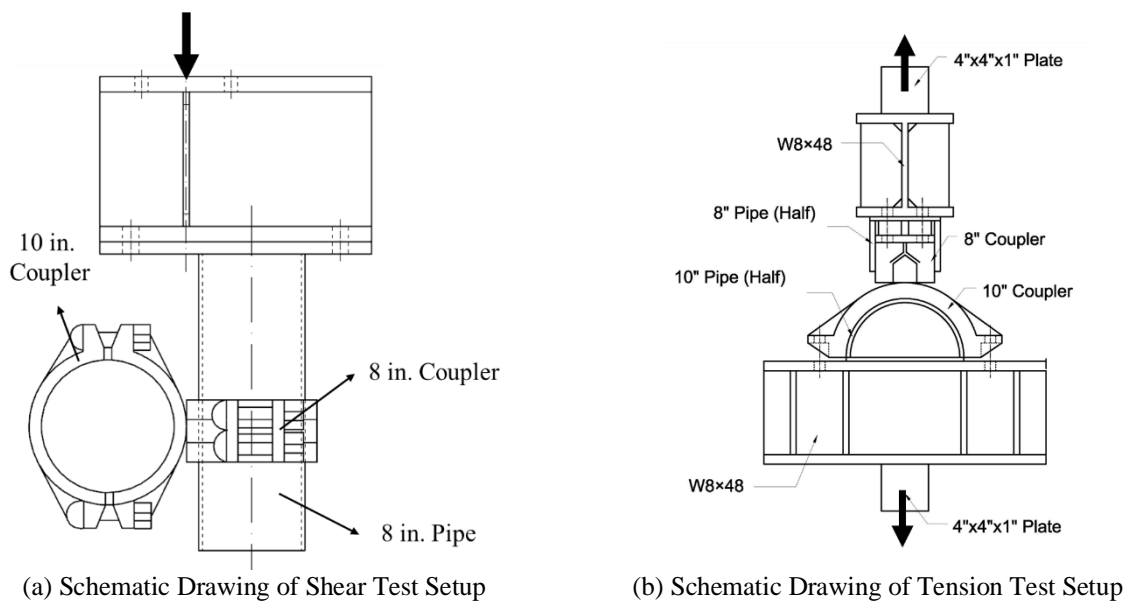


Figure 17. Schematic Drawings of Test Setups

For the tension test setup, a half-coupler setup was adopted, as shown in Figure 17(b). The interior two half-couplers riveted together were bolted onto a loading rig mounted in a servo-controlled universal testing machine. Half-pipes were also installed inside the couplers to provide correct boundary conditions. The half-pipes were cut to be a little deeper than the radius of the coupler such that the coupler would not bear against the loading rig.

A torque wrench was used to apply 300 ft·lb on each bolt as designated in KDOT's plan drawings. When tightening the bolts in the tension test setup, at least one side of the jig on the loading machine was released to prevent tensioning the rivet before loading.

As shown in Figure 18, the pipes and couplers used in the shear test setup were marked before fatigue testing to capture any sliding/slip between them.



(a) Markers on Horizontal Pipe



(b) Markers on Vertical Pipe

Figure 18. Shear Test Setups Marked to Capture Sliding between Coupler and Pipe

3.2 Testing Plan

Twenty-two specimens were tested in total, including 13 in tension, 5 in vertical shear, and 4 in horizontal shear. The coupler assemblies and pipes used in the test program were obtained from Steve Johnson Fabrication, Inc., which is the company that manufactures the majority of OHTSS in Kansas.

A summary of the testing plan is presented in Table 4. In addition to the tests listed in Table 4, two additional coupler connections from a KDOT OHTSS taken out of service were tested in tension at a stress range of 26.6 ksi to serve as trial runs at the beginning of the experimental study. The stress range was calculated based on the area of the rivet, which is 0.601 in^2 , since the nominal diameter of the rivet is $7/8 \text{ in}$. A minimum load of 0.5 kip was used in all the tests to ensure all applied loading was tensile.

The majority of the tension specimens were tested at a frequency of 5 Hz, selected to allow an acceptable testing time while maintaining a stable loading protocol. The exceptions were two specimens tested at 4.2 ksi; a frequency of 8 Hz was adopted for these tests as the tests were expected to require many millions of cycles (>20 million) to complete. All shear specimens were tested at 4 Hz.

Specimens were inspected multiple times a day during testing to determine any visible damage. For specimens expected to require millions of load cycles, testing was conducted 24 hrs per day. Inspections were not performed during overnight hours.

Table 4. Fatigue Testing Matrix

Loading	Number of Specimens Tested	Stress Range	Setup
Tension	13	1 at 26.6 ksi 1 at 15.1 ksi 2 at 10.5 ksi 3 at 8.3 ksi 4 at 5.8 ksi 2 at 4.2 ksi	Half-couplers were bolted onto a loading rig in the universal testing frame. Cyclic loading applying direct tension in the rivet was applied. This loading condition captured tensile stresses produced by out-of-plane shear induced by natural wind.
Vertical shear	5	2 at 10.8 ksi 1 at 9.1 ksi 1 at 7.5 ksi 1 at 5.0 ksi	The 8-in. diameter pipe (truss chord) was installed in the horizontal position. The 10-in. diameter pipe (pole) was in the vertical position. Loads were applied vertically. This loading represents in-plane shear such as those induced by truck gust loading.
Horizontal shear	4	1 at 10.8 ksi 1 at 9.1 ksi 1 at 7.5 ksi 1 at 5.0 ksi	The 10-in. diameter pipe (pole) was installed in the horizontal position. The 8-in. diameter pipe (truss chord) was in the vertical position. Loads were applied vertically. This loading represents the condition in which the truss chord is loaded axially.

Experimental Program Results & Discussion

In this study, 22 coupler connection specimens were tested under three modes of loading: tension, vertical shear, and horizontal shear. The following sections discuss the performance of the coupler connection for these three loading conditions, and presents the results in the context of the demands on the coupler as determined through finite element analysis.

4.1 Rivet Loaded in Shear

All the specimens loaded in shear (both horizontal and vertical shear modes) were loaded at stress ranges between 5.0-10.8 ksi, which is significantly greater than the design-level fatigue demands predicted from the finite element analysis. All specimens tested in horizontal shear and four of the five specimens tested in vertical shear experienced runout. *Runout* means that the number of cycles applied in the test was greater than that corresponding to the ‘knee point’ for the corresponding fatigue category without any damage being detected in the component, implying the specimen has exhibited infinite fatigue life. In design, one can assume that fatigue failure will not occur if loaded below the constant amplitude fatigue life (CAFL) threshold for that category.

As shown in Figure 19, for the mode in which the rivet was loaded in horizontal shear, the specimens all experienced runout when tested at multiple stress ranges. The test conducted at the highest stress range achieved runout at a Category C load level. The maximum horizontal shear demand on the coupler connection from the finite element analyses was approximately 0.5 kip, which corresponds to a stress range of ~0.8 ksi in the rivet. Therefore, the experimental results all significantly out-performed this level of demand.

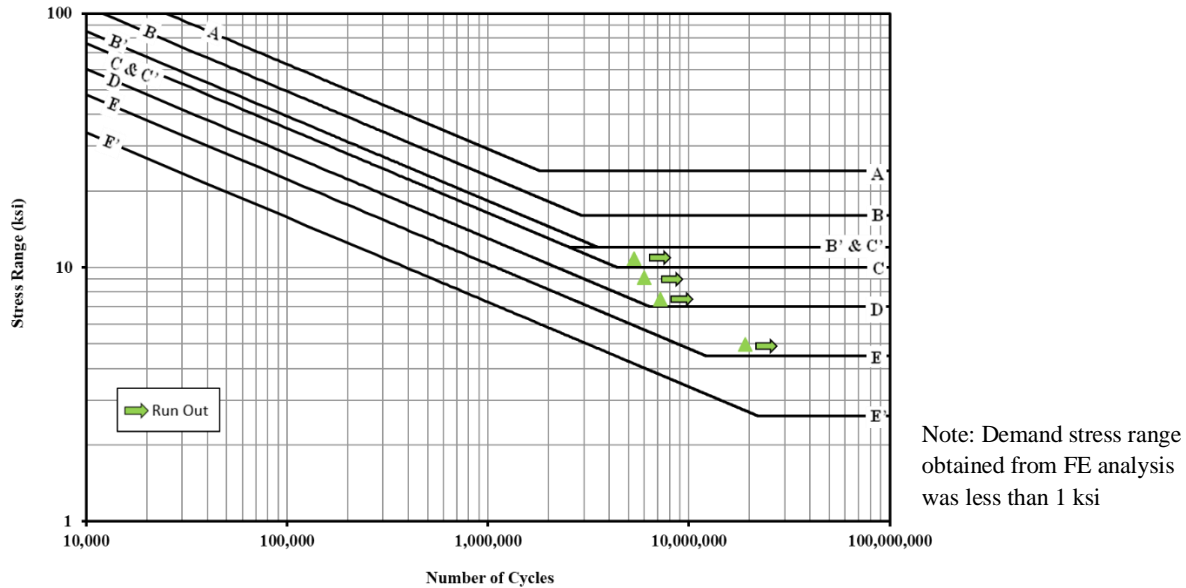


Figure 19. S-N Curve – Coupler Connection Rivet Loaded in Horizontal Shear

Five specimens were tested in vertical shear. Four of them experienced runout. Only one specimen failed at approximately 2 million cycles under a stress range of 10.8 ksi. However, the horizontal aluminum pipe cracked during this test and experienced some rotation under the applied load; therefore, the rivet failed in a combined shear and bending mode. This specimen was treated as an outlier since bending was not supposed to occur in the test and is not expected to occur in service. This data point is not presented in Figure 20, which shows the fatigue results for couplers loaded in vertical shear overlaid on the AASHTO S-N curves. Another specimen was tested under the same stress range after repairing the cracked test setup, and it experienced runout. The four remaining data points for the vertical shear loading condition were conducted at different stress ranges between 5.0-10.8 ksi; the specimen that was tested at the highest stress range performed above a Category C level. The stress range obtained in FE analyses is shown as the red line in Figure 20. The calculated demand stress range is much lower than any of the specimens tested.

It should be noted that no sliding between couplers and pipes or loosening of bolts were observed in any of the tests.

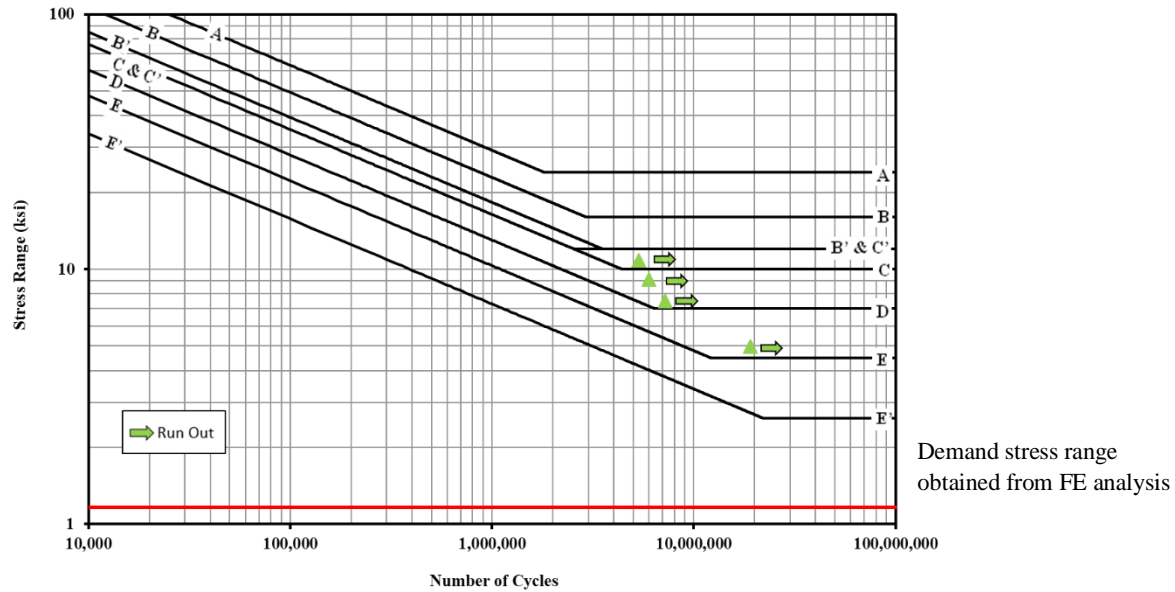


Figure 20. S-N Curve – Coupler Connection Rivet Loaded in Vertical Shear

4.2 Rivet Loaded in Tension

Thirteen specimens were tested such the rivet connecting the two interior couplers was loaded in tension. This fatigue testing protocol was intended to represent the tensile response in the rivet from out-of-plane shear induced by natural wind gust loading, and was the most significant demand the coupler connections experienced according to the results of the finite element analyses.

The S-N curve showing the results from 13 fatigue tests is presented in Figure 21. It does not include the two specimens from OHTSS taken out of service, tested at 26.6 ksi. Four of the 13 specimens fell below the Category E' curve. Three of them were in the region where the stress range was larger than 10 ksi. Data points mostly fell above the Category E' curve when the stress range was smaller than 10 ksi. Only one of nine specimens tested at stress ranges less than 10 ksi fell below Category E'. Both specimens tested at 4.2 ksi experienced runout (the two data points are overlaid with each other in Figure 21).

For specimens tested at the higher stress range (>10 ksi), failures were characterized by cracking occurring in either the 10-in. coupler or the 8-in. coupler. The two specimens from structures taken out-of-service (not presented in Figure 21) also failed by cracking of the 10-in. coupler. Both rivet failures and coupler failures were observed as occurring in specimens tested

under lower stress ranges (<10 ksi). In fact, two specimens tested at 8.3 ksi failed in a combined mode, in which damage was observed in both the rivet and coupler upon failure.

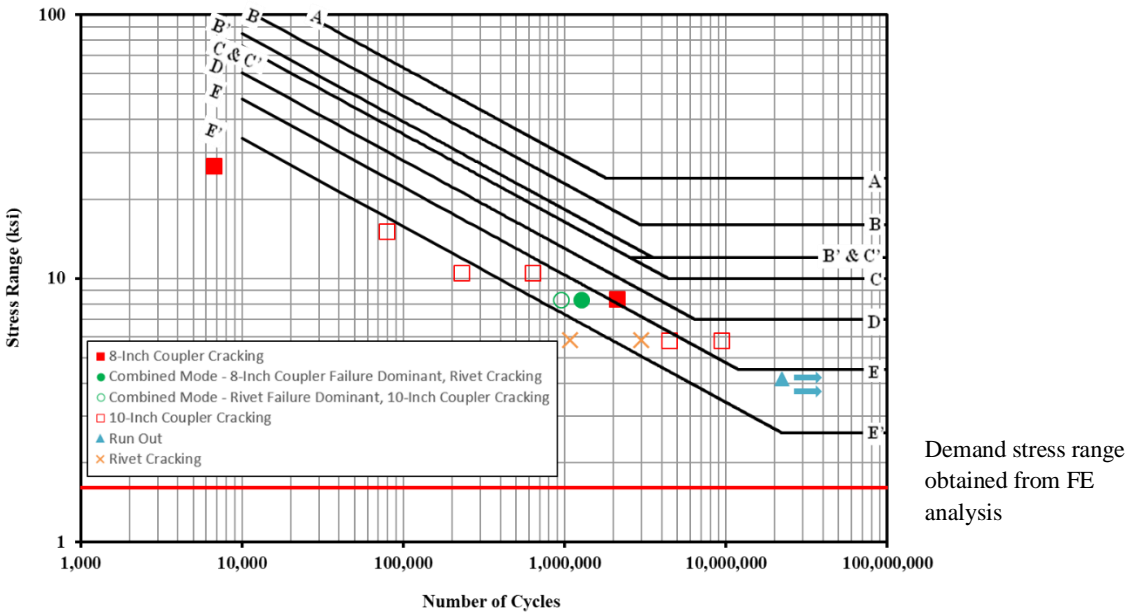


Figure 21. S-N Curve – Coupler Connection Rivet Loaded in Tension

As shown in Figure 21, specimens tested in tension failed in four different manners:

1. Cracking in the 8-in. coupler,
2. Cracking in the 10-in. coupler,
3. Combined mode in which damage occurred in both the coupler and rivet,
- and
4. Cracking in the rivet.

The details of each test are provided in the following sections.

4.2.1 Specimens tested at 26.6 ksi:

4.2.1.1 *FAT-TENS(USED)1*: This specimen was one of the couplers from an OHTSS taken out of service, and thus had accumulated prior fatigue damage over a life of service. It was one of the first specimens tested as part of this research program and was loaded at a high stress range. The specimen failed at approximately 3,000 cycles. The failure occurred by a rapid fracture of the

10-in. coupler, in a brittle manner. There were no warning signs before the fracture. The photographs of the coupler after failure are presented in Figure 22.



(a) Failure of FAT-TENS(USED)1



(b) Cracked 10-in. Coupler

Figure 22. Failure of FAT-TENS(USED)1 Tested at 26.6 ksi

Some corrosion products were observed on the failure surface, as shown in Figure 22. This raised some concern whether there may have been pre-existing cracks before testing. The surface was examined under a microscope. The results were not conclusive. Section 8 of the report discusses more details regarding this topic.



Figure 23. Failure Surface of FAT-TENS(USED)1

4.2.1.2 FAT-TENS(USED)2: This specimen was also one from a structure taken out of service, and thus also had previously accumulated a lifetime of fatigue cycles. The specimen was tested at a high stress range of 26.6 ksi, and failed at 10,581 cycles. The failure mode was cracking of the 10-in. coupler. Photographs showing the specimen after failure are presented in Figure 24.



(a) Failure of FAT-TENS(USED)2



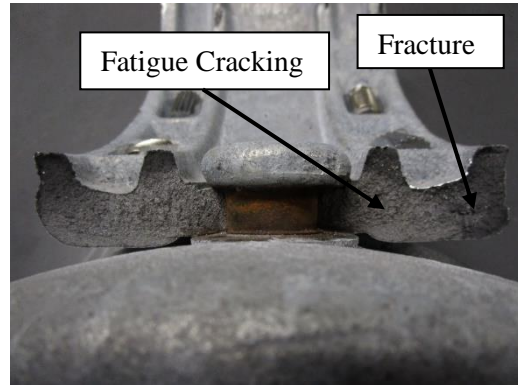
(b) Failure Surface of FAT-TENS(USED)2

Figure 24. Failure of FAT-TENS(USED)2 Tested at 26.6 ksi

4.2.1.3 *FAT-TENS1*: *FAT-TENS1* was a new “off-the-shelf” coupler, tested at a high stress range of 26.6 ksi. Failure occurred in a brittle manner at 6,708 cycles. The 8-in. coupler broke into half at the position of the rivet hole in a brittle fashion, without no noticeable signs of distress before failure. After the test was concluded, the failure surface was inspected and two regions were identified: a smoother and brighter region, and a coarser and darker region. The smoother region was created during fatigue crack propagation, and the coarser region was the result of fracture. The failure surface indicated that cracks initiated at the rivet hole and propagated perpendicular to the tensile bending stress in the coupler. These two regions can be clearly seen in most of the specimens for which failures were characterized by cracking of the coupler.



(a) Failure of FAT-TENS1



(b) Failure Surface of FAT-TENS1

Figure 25. Failure of FAT-TENS1 Tested at 26.6 ksi

4.2.2 Specimens tested at 15.1 ksi:

4.2.2.1 *FAT-TENS13*: *FAT-TENS13* was a new “off-the-shelf” coupler, tested at 15.1 ksi. The specimen failed at 78,818 cycles, characterized by brittle cracking of the 10-in. coupler. Inspections were regularly performed during testing, but no cracks were observed before failure. Photographs of the specimen after failure are presented in Figure 26.



(a) Failure of *FAT-TENS13*



(b) Failure Surface of *FAT-TENS13*

Figure 26. Failure of *FAT-TENS13* Test at 15.1 ksi

The graph of the assembly stiffness versus the number of applied cycles is presented in Figure 27. The stiffness started to reduce at approximately 30,000 cycles and then began to rapidly decrease at approximately 750,000 cycles. However, despite regular inspections, cracks were not observed until complete failure of the coupler.

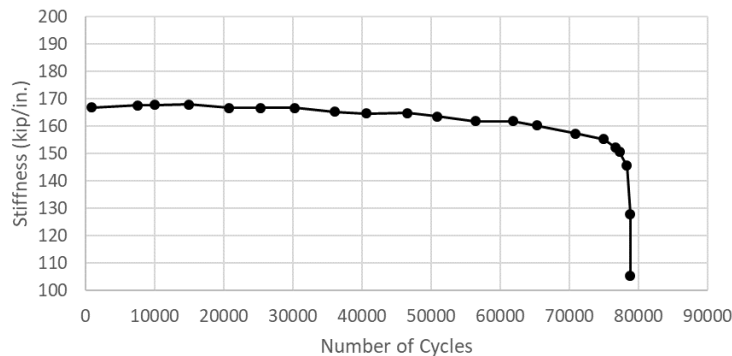


Figure 27. Stiffness vs. Number of Cycles for *FAT-TENS13* Tested at 15.1 ksi

4.2.3 Specimens tested at 10.5 ksi:

4.2.3.1 *FAT-TENS11*: *FAT-TENS11* was a new “off-the-shelf” coupler tested at 10.5 ksi. During an inspection at 195,754 cycles, it was observed that the stiffness of the assembly decreased, but no crack was observed. Over the next 3,000 cycles, stiffness continued decreasing but there was still no visible damage. At 228,327 cycles, a crack was identified as having propagated in the 10-in. coupler wall, extending through approximately 2/3 of it. After another 55 cycles, the 10-in. coupler broke in half. The final failure occurred at 228,382 cycles. Photographs of the specimen after failure are shown in Figure 28.



(a) Failure of *FAT-TENS11*



(B) Failure Surface of *FAT-TENS11*

Figure 28. Failure of *FAT-TENS11* Tested at 10.5 ksi

Figure 29 presents assembly stiffness with respect to the number of applied cycles. Stiffness started to decrease at approximately 150,000 cycles. However, when the researcher observed the crack, it was only 55 cycles away from failure.

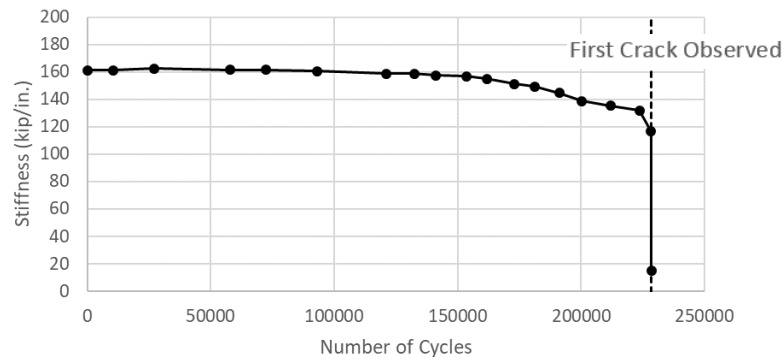


Figure 29. Stiffness vs. Number of Cycles for *FAT-TENS11* Tested at 10.5 ksi

4.2.3.2 *FAT-TENS12*: *FAT-TENS12* was a new “off-the-shelf” coupler, tested at 10.5 ksi. During an inspection performed at 632,420 cycles, a thin crack was found on one side of the 10-in. coupler. The crack had not yet propagated through the thickness of the coupler. After another 323 cycles, the 10-in. coupler broke in half. The final failure occurred at 632,743 cycles. Photographs of the specimen are presented in Figure 30.

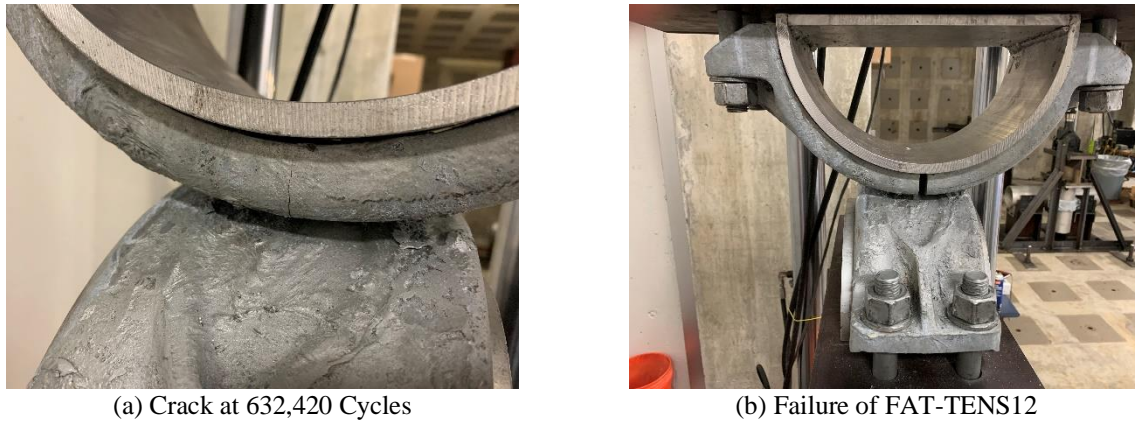


Figure 30. Failure of *FAT-TENS12* Tested at 10.5 ksi

The record of assembly stiffness during testing is shown in Figure 31. The stiffness started to reduce slightly at approximately 450,000 cycles, but did not change much before it started to decrease rapidly at approximately 600,000 cycles. When the first crack was observed, it was still thin but the coupler was only 323 cycles away from failure.

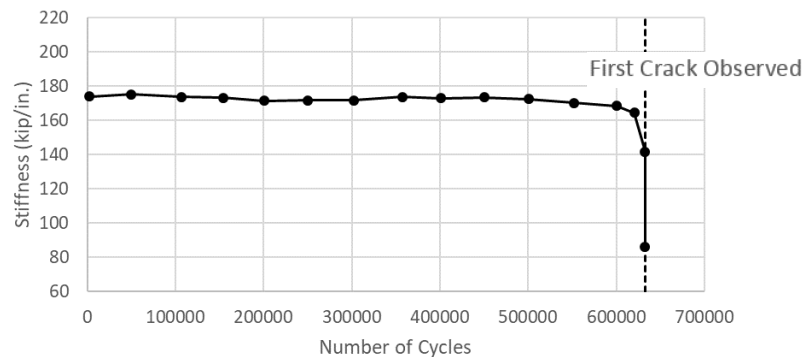


Figure 31. Stiffness vs. Number of Cycles for *FAT-TENS12* Tested at 10.5 ksi

4.2.4 Specimens tested at 8.3 ksi:

4.2.4.1 *FAT-TENS2*: *FAT-TENS2* was a new “off-the-shelf” coupler, tested at 8.3 ksi. The specimen failed by rivet cracking at 952,738 cycles. No visible signs of damage were observed before failure. As shown in Figure 32(a), cracking occurred at the intersection of the rivet head and shank, at the side connecting to the 10-in. coupler. After uninstalling and inspecting the specimen, a crack was also observed on the 10-in. coupler as shown in Figure 32(b). The failure of this specimen was classified as a combined mode, since both of the coupler and the rivet were damaged.



(a) Rivet Cracking



(b) Crack on the 10-in. Coupler

Figure 32. Failure of *FAT-TENS2* Tested at 8.3 ksi

4.2.3.2 *FAT-TENS3*: *FAT-TENS3* was a new “off-the-shelf” specimen, tested at 8.3 ksi. The final failure of the specimen occurred at 1,263,601 cycles, and was classified as a combined mode. At 1,263,000 cycles, the 8-in. coupler wall cracked on one side. Fatigue loading was continued, and the other side of the 8-in. coupler wall cracked after another 600 cycles. Upon specimen removal and inspection, a crack was observed on the rivet at the intersection of the rivet head and shank, on the side that was connected to the 8-in. coupler. The crack had propagated more than halfway through the rivet. Photographs of the specimen after failure are presented in Figure 33.



(a) Coupler Cracking



(b) Rivet Cracking

Figure 33. Failure of FAT-TENS3 Tested at 8.3 ksi

The load and displacement are shown in Figure 34. The stiffness of the coupler assembly started to decrease at approximately 950,000 cycles, but no visible fatigue damage was observed until half of the 8-in. coupler cracked at 1,263,000 cycles. An additional 600 cycles led to complete failure of the coupler.

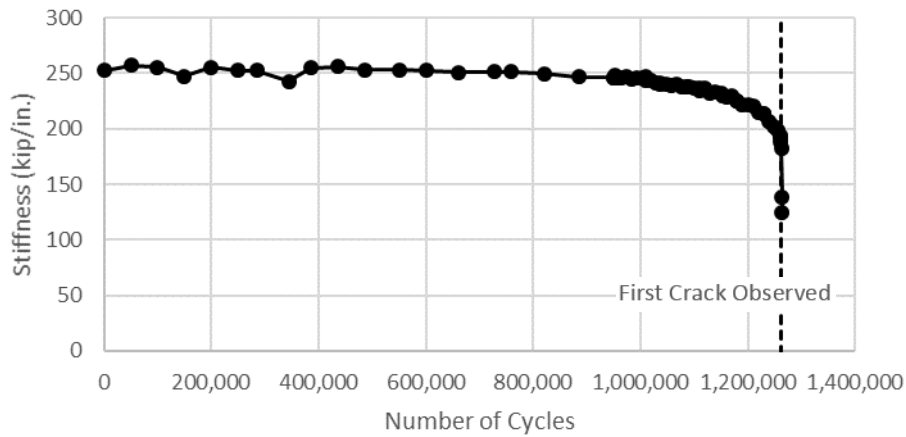


Figure 34. Stiffness vs. Number of cycles for FAT-TENS3 Tested at 8.3 ksi

4.2.3.3 FAT-TENS9: FAT-TENS9 was a new “off-the-shelf” coupler tested at a stress range of 8.3 ksi. The test was stopped at 2,124,128 cycles when cracking of the 8-in. coupler triggered the displacement interlock of the loading machine. A crack was found to have propagated through-thickness on one side of the coupler. On the other side, the crack propagated to the edge of the coupler but had not yet propagated through-thickness. Photographs of the specimen after failure are presented in Figure 35.



(a) Crack on One Side Cut Through the Thickness



(b) Crack on the Other Side Propagated to the Edge

Figure 35. Failure of FAT-TENS9 Tested at 8.3 ksi

The record of coupler assembly stiffness during the test is presented in Figure 36. The last inspection performed before failure was at approximately 1.9 million cycles. Although the stiffness of the assembly started to decrease at approximately 1.6 million cycles, no visible cracks were observed in the last inspection.

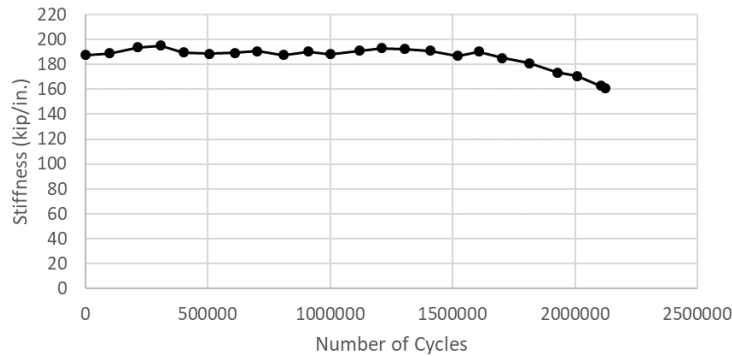


Figure 36. Stiffness vs. Number of Cycles for FAT-TENS9 Tested at 8.3 ksi

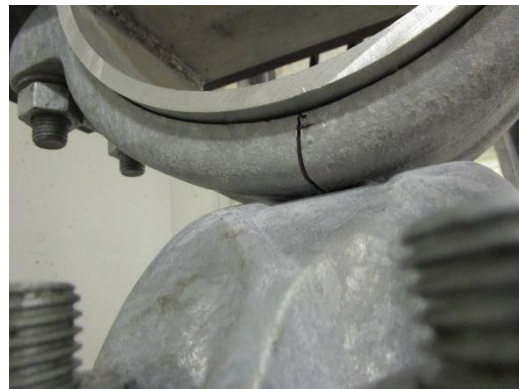
4.2.5 Specimens tested at 5.8 ksi:

4.2.5.1 *FAT-TENS4*: *FAT-TENS4* was a new “off-the-shelf” coupler, tested at a stress range of 5.8 ksi. Final failure was observed as occurring at 9,405,564 cycles, characterized by cracking

of the 10-in. coupler. At 7,214,300 cycles, a crack was observed on half of the 10-in. coupler, as shown in Figure 37(a). At 7,433,422 cycles, the crack propagated through the thickness of the 10-in. coupler. An inspection was performed at 9,327,091 cycles. No other crack was observed besides the aforementioned one, however, it was observed that the crack had become wider, as shown in Figure 37(b). Complete failure occurred at 9,405,564 cycles, and the test was terminated after the crack propagated through the other half of the 10-in. coupler. A photograph of the specimen after failure is presented in Figure 38.



(a) Crack at 7,214,300 Cycles



(b) Crack at 9,327,091 Cycles

Figure 37. Cracking of FAT-TENS4 Tested at 5.8 ksi



Figure 38. Failure of FAT-TENS4 Tested at 5.8 ksi

The stiffness record for FAT-TENS4 is presented in Figure 39. In this test, the first crack was detected at about 7.2 million cycles, and it took an additional 2 million cycles to reach complete failure. This was different than other tests, since in most of the tests cracks were not visually-observable until complete failure was imminent.

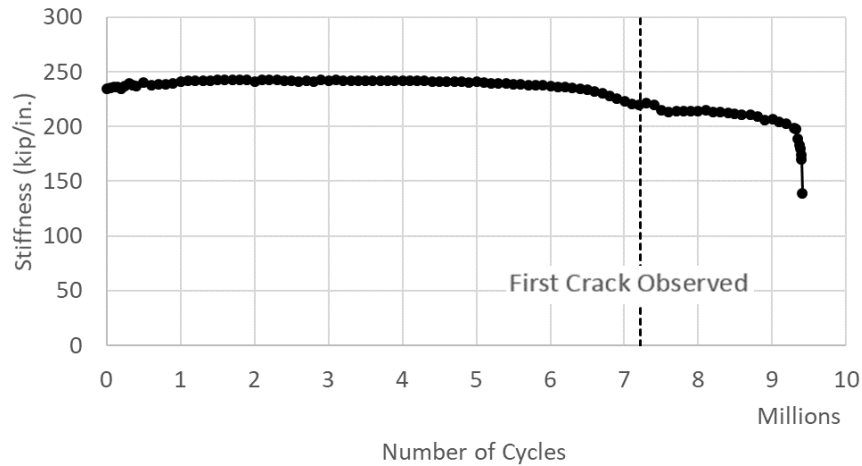


Figure 39. Stiffness vs. Number of Applied Cycles for FAT-TENS5 Tested at 5.8 ksi

4.2.5.2 *FAT-TENS5*: *FAT-TENS5* was a new “off-the-shelf” coupler, tested at a stress range of 5.8 ksi. Failure occurred at 4,453,581 cycles, characterized by the 10-in. coupler cracking in half. In the last inspection performed at 4,432,960 cycles, a decrease of stiffness was observed but no visible crack was identified. Photographs of the specimen after failure are presented in Figure 40.

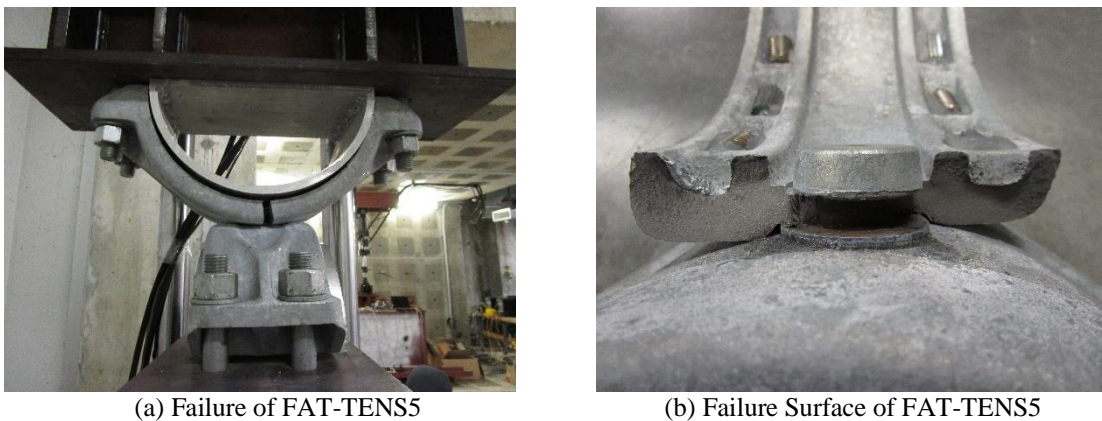


Figure 40. Failure of FAT-TENS5 Tested at 5.8 ksi

The stiffness record for *FAT-TENS5* is presented in Figure 41. Although stiffness of the assembly started to decrease at approximately 3.2 million cycles, no cracking was observed until complete failure occurred.

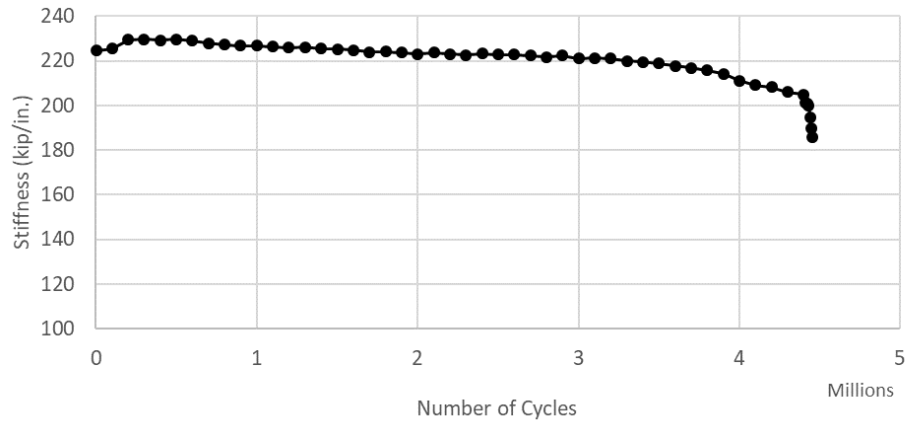


Figure 41. Stiffness vs. Number of Cycles for FAT-TENS5 Tested at 5.8 ksi

4.2.5.3 *FAT-TENS7*: *FAT-TENS7* was a new “off-the-shelf” coupler, tested at a stress range of 5.8 ksi. The specimen failed by cracking of rivet, with failure occurring at 2,961,381 cycles. Although inspection was performed regularly, no visible damage was observed until failure. Photographs of the specimen after failure are shown in Figure 42.



(a) Failure of *FAT-TENS7*



(b) Failure Surface of *FAT-TENS7*

Figure 42. Failure of *FAT-TENS7* Tested at 5.8 ksi

The stiffness record for *FAT-TENS7* is shown in Figure 43. No gradual decrease in stiffness was observed as occurring in this test.

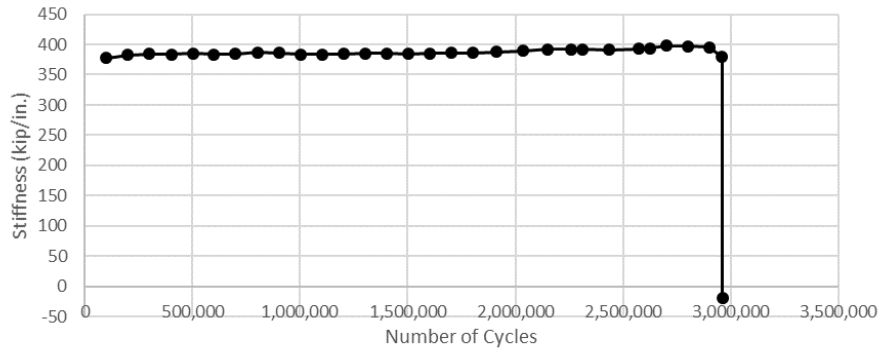


Figure 43. Stiffness vs. Number of Cycles for FAT-TENS7 Tested at 5.8 ksi

4.2.5.4 *FAT-TENS8*: *FAT-TENS8* was a new “off-the-shelf” coupler, tested at a stress range of 5.8 ksi. The specimen failed by cracking of rivet at 1,080,756 cycles. No visible damage was observed before failure. Photographs of the specimen after failure are shown in Figure 44.



Figure 44. Failure of FAT-TENS8 Tested at 5.8 ksi

The stiffness record for *FAT-TENS8* is shown in Figure 45. Similar to the behavior observed for *FAT-TENS7*, reductions in stiffness were not observed as occurring before failure.

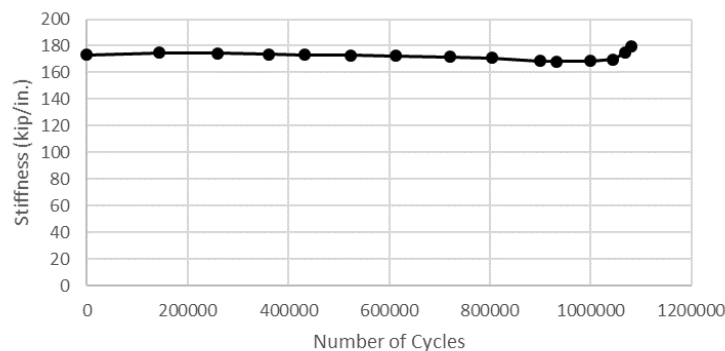


Figure 45. Stiffness vs. Number of Cycles for FAT-TENS8 Tested at 5.8 ksi

4.2.6 Specimens tested at 4.2 ksi:

Two specimens, FAT-TENS6 and FAT-TENS10, were tested at the stress range of 4.2 ksi. Both were new “off-the-shelf” couplers, and both experienced runout. The specimens were loaded for more than 22.5 million cycles, which was beyond the knee point of the Category E’ curve on the AASHTO S-N diagram. Inspections were performed regularly, and no fatigue crack damage was observed. An analysis of load and displacement data also indicated that connection stiffness did not decrease during the test for either specimen.

4.3 Discussion of Tension Test Results

Among the 11 new “off-the-shelf” coupler assemblies that experienced failure in the tension tests, eight of them failed in a mode of coupler cracking (including the one failed in a combined mode with coupler cracking the dominant mode), and three failed by rivet cracking (including one that failed in a combined mode with rivet cracking dominant). Among the eight with failures characterized by coupler cracking, it was the 10-in. coupler cracked in five of the tests. This result was not unexpected, given that the 10-in. couplers have a longer span than the 8-in couplers. However, given that the 8-in. coupler was the component that experienced failure in three of the specimens, small pre-existing flaws could be a factor affecting the failure mode.

Rivet cracking did not occur in couplers tested under relatively large stress ranges (>10 ksi). For specimens tested under smaller stress ranges (<10 ksi), rivet cracking occurred in three out of the seven specimens that experienced failure.

The stiffness records indicated that for most of the specimens experiencing coupler cracking, stiffness remained constant and then gradually decreased until final failure was reached. When the specimen was close to failure, reduction in stiffness accelerated. For specimens that experienced rivet cracking, however, no noticeable changes in the stiffness record were apparent before failure occurred.

All specimens were inspected multiple times a day during testing. Specimens that exhibited long fatigue lives were cycled 24 hrs/day, and inspections were not conducted during overnight hours. Nonetheless, even specimens for which failure occurred during daytime hours, cracks were

generally only identifiable when the specimen was very close to failure. In some of them, cracks were not observed at all before failure, despite the fact that inspection was regularly performed. The configuration of the coupler assembly, in which the two interior couplers are riveted together, impeded the inspection of cracks. Cracking was only visible once it grew out of the overlapping region where the two couplers were connected.

Four off-the-shelf specimens tested at a level below Category E' under tensile fatigue loading. Three of them were tested at stress ranges greater than 10ksi. Two specimens tested at 4.2 ksi experienced runout. This established two data points for tensile fatigue performance above the constant fatigue threshold of the Category E', which is 2.6 ksi. These two specimens were tested at a stress range much larger than what obtained from the finite element analyses of OHTSS under design loads, which was only 1.7 ksi. Based on these findings, it appears that the coupler connection at least meets Category E' behavior for very low tensile stress ranges. Although Category E' details are characterized by poor fatigue performance, due to very low anticipated stress ranges in service, tensile fatigue failures are not considered likely to occur in the coupler connections used in OHTSS.

It should also be noted that out-of-plane responses in the truss were more significant than in-plane responses, and the fatigue resistance of the coupler assemblies in the vertical shear direction (corresponding to the truss in-plane response) was much better than in tension (corresponding to the truss out-of-plane response). Because of the smaller fatigue demands on the couplers in horizontal and vertical shear (based on the FEA performed in this study) and greater fatigue resistance under these loading modes than in tension, shear forces induced on the couplers by truck-induced gust and natural wind gust are not expected to produce fatigue concerns.

If any cracks should ever be found in an in-service coupler assembly, it is recommended that it be replaced as quickly as possible - no matter how small the cracks are - since in the lab cracks were only ever observable when the assembly was close to failure.

4.4 Identifying Pre-Existing Cracks in Used Coupler

As discussed, tensile fatigue tests were conducted on two coupling assemblies extracted from OHTSS taken out-of-service. Corrosion products were found on the failure surfaces, which

raised questions regarding whether there may have been existing fatigue cracks that developed while the couplers were in service. After fatigue testing was conducted in the laboratory at KU, the failure surfaces were examined under a microscope. However, the microscopic photographs (Figure 46) were found to be inconclusive. Corrosion products were also found on the failure surface of some newly fabricated specimens which had been sitting in the lab for a few months. Figure 47 presented the failure surface of FAT-TENS4. Corrosion products were found on the surface. The two couplers were riveted before galvanizing. There was no zinc in the gap between the rivet shank and the washer. Corrosion products were found in all the specimens at the gaps. When a coupler failed, it is very possible that the corrosion products migrated to the surface from the gap due to the violent vibrations caused by the fracture.



(a) Fracture Surface of FAT-TENS(USED)1



(b) Microscopic Photograph of FAT-TENS(USED)1

Figure 46. Failure Surface of Microscopic Photograph of FAT-TENS(USED)1



Figure 47. Corrosion Products on Failure Surface of FAT-TENS4

4.5 Confirmation of Coupler Material

To determine the material composition of the coupler connections, a sample was cut from one of the couplers taken from an out-of-service OHTSS and sent to a materials testing laboratory. The material test was performed by Pacific Testing Laboratories, Inc., Valencia, CA. Figure 48 shows a photomicrograph showing the microstructure of the material sample. Graphite nodules in a matrix of α -ferrite (with some pearlite) were observed. The microstructure is characteristic of ductile cast irons.

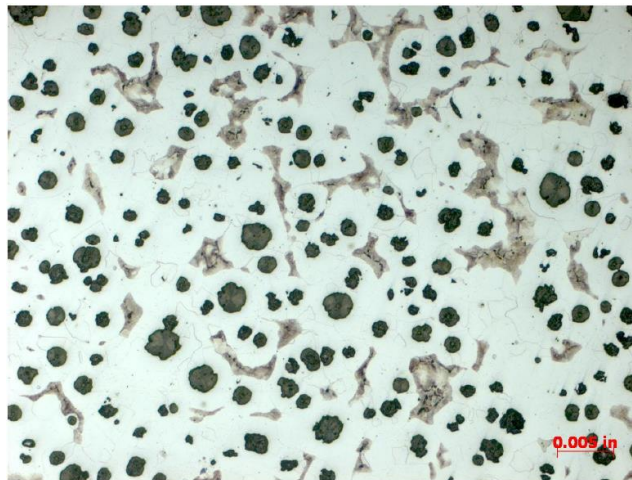


Figure 48. Photomicrograph of Coupler Material Sample

4.6 Experimental Test Program Conclusions

In this study, 22 newly fabricated coupler assemblies were tested, among which 13 were tested in tension, four were tested in horizontal shear, and five were tested in vertical shear. An additional two assemblies from structures taken out of service were tested in tension as trial runs at the beginning of the testing program. Conclusions from the experimental test program are as follows:

- Coupler connections tested in horizontal shear and vertical shear all experienced runout. None of the shear tests produced observable damage in the rivet or coupler assembly, nor was any sliding/slip observed between the pipe and coupler. Specimens tested in shear modes were subjected to stress ranges between 5.0-10.8 ksi, which is significantly higher than the design-level stress range demands predicted from finite element analyses. Based on these findings,

the coupler connection is not considered to be at-risk of premature fatigue failure under shear demands.

- Coupler connections tested in tension were subjected to stress ranges between 4.2-26.6 ksi. The results of the tensile fatigue tests showed data centered around the Cat E' curve, but seemingly with a lower slope. The data tended to out-perform Category E' for lower values of stress range (<10 ksi) when loaded in tension, but did not meet Cat E' for higher stress ranges. Nonetheless, predicted design-level fatigue demands on the coupler are expected to be very low, approximately 1.7 ksi. Based on the experimental data gathered as part of this study, the results appear to indicate that the coupler's resistance exceeds the fatigue demands placed upon it in usual design/service applications.
- Coupler assemblies tested in tension experienced failure modes that included: 10-in. coupler cracking, 8-in. coupler cracking, rivet cracking, and combined modes of coupler cracking and rivet cracking. Rivet cracking was not observed in tests conducted for stress ranges greater than 10 ksi. Additionally, cracking in the 10-in. coupler was more commonly observed than cracking in the 8-in. coupler. Failures that were characterized by rivet cracking were not inspectable before complete failure, as the configuration of the two interior couplers impeded inspection. Additionally, fatigue cracks in the coupler housings were not observable until they had propagated significantly and the connection was close to complete failure.

Conclusions and Recommendations

In this study, twenty-two coupler assemblies were tested at the University of Kansas in three loading modes: 1) rivet loaded in tension, 2) rivet loaded in vertical shear, and 3) rivet loaded in horizontal shear. The test setups were developed by drawing upon the findings from a series of finite element analyses of OHTSS under design-level fatigue loadings. The analyses included four Kansas DOT OHTSS each having a different span length and subjected to six loading modes. The major conclusions of the study are summarized here.

- Behavior of coupler connections in bridge-type overhead truss sign structures was found to be similar to that of pinned connections. The coupler connections have little to no capability to transfer moment and are essentially subjected to direct tension and shear.
- Among all cases, the maximum out-of-plane shear, in-plane shear, and axial force were found to be approximately 1 kip, 0.7 kip, and 0.5 kip, respectively (1.7 ksi, 1.2 ksi, and 0.8 ksi with respect to the rivet cross-sectional area), from the finite element analyses. Other load components were negligible.
- For all modes of fatigue loading applied in the lab (vertical shear on the rivet, horizontal shear on the rivet, and tension on the rivet), the fatigue resistance was found to out-perform demands determined from FEA. The resistances of the coupler connection in both shear modes significantly exceeded demands. While the resistance of the coupler connection in tension was significantly lower, the coupler still exhibited performance about the Category E' CAFL, which was greater than the predicted demands in tension.
- Fatigue cracks were not inspectable until failure was imminent. In fact, cracking was not observable at all before complete fatigue failure occurred.
- The study did not find reliable evidence of pre-existing cracks in two coupler assemblies extracted from structures taken out of service.

References

- AASHTO. (2009). Standard Specifications for Structural Supports for Highway Signs, Luminaires and Traffic Signals. (5th ed.). American Association of State Highway Transportation Officials, Washington, D.C.
- Dexter, R.J. and Ricker, M.J. (2002). NCHRP Report 469: Fatigue-Resistant Design of Cantilevered Signal, Sign, and Light Supports. Transportation Research Board of the National Academies, Washington, D.C.
- Foley, C.M., Ginal, S.J., Peronto, J.L., and Fournelle, R.A. (2004). Report 04-03: Structural Analysis of Sign Bridge Structures and Luminaire Supports. Marquette University, Milwaukee, WI.
- Fouad, F.H., Davidson, J.S., Delatte, N., Calvert, E.A., Chen, S., Nunez, E., and Abdalla, R. (2003). NCHRP Report 494: Structural Supports for Highway Signs, Luminaires, and Traffic Signals. Transportation Research Board of the National Academies, Washington, D.C.
- Foutch, D.A., Rice, S.A., Lafave, J.M., Valdovinos, S., and Kim, T.W. (2006). FHWA/IL/PRR 153: Evaluation of Aluminum Highway Sign Trusses and Standards for Wind and Truck Gust Loadings. Illinois Department of Transportation, Springfield, Illinois.
- Kacin, J., Rizzo, P., and Tajari, M. (2010). "Fatigue Analysis of Overhead Sign Support Structures." *Engineering Structures*, 32(6), 1659–1670.
- Kaczinski, M.R., Dexter, R.J., and Van Dien, J.P. (1998). NCHRP Report 412: Fatigue-Resistant Design of Cantilevered Signal, Sign and Light Supports. Transportation Research Board of the National Academies, Washington, D.C.
- McCullom, B.F. (1973). Report K-F-72-3: Testing of Overhead Sign Support Truss to End-Support Connections. State Highway Commission of Kansas, Topeka, Kansas.
- McLean, T.W., Park, J.S., and Stallings, J.M. (2004). Fatigue Evaluation of Two Variable Message Sign Structures, Alabama Department of Transportation, Montgomery, Alabama.
- Mirza, J.F., Tung, C.C., and Smith, J.C. (1975). Static and Dynamic Behavior of Trichord Truss' Overhead Sign Support Structures. North Carolina State University, NC.
- Munse, W.H., and Cox, H.L. (1956). The Static Strength of Rivets Subjected to Combined Tension and Shear. *University of Illinois Bulletin*, Urbana, Illinois.

APPENDIX A1 Loads Applied in FE Models

Table A1-1. Loads Applied in Model of 60 ft Overhead Truss Sign Structure

	NWB	NWF	NWS		TGL	TGM	TGR
Supporting Frame Pipe	0.00047 (kip/in)		Below Truss	0.00065 (kip/in)			
			Above Truss	0.0013 (kip/in)			
Truss Chord	0.00071 (kip/in)	0.00063 (kip/in)			0.0027 (kip/in)		
Sign Beam	0.00022 (kip/in)						
Sign 1	0.000043 (ksi)						
Sign 2	0.000041 (ksi)						
Walkway Beam					0.00078 (kip/in)		

Table A1-2. Loads Applied in Model of 83 ft Overhead Truss Sign Structure

	NWB	NWF	NWS		TGL	TGM	TGR
Supporting Frame Pipe	0.00047 (kip/in)		Below Truss	0.00063 (kip/in)			
			Above Truss	0.0012 (kip/in)			
Truss Chord	0.00071 (kip/in)	0.00063 (kip/in)			0.0027 (kip/in)		
Sign Beam	0.00022 (kip/in)						
Sign	0.000043 (ksi)						
Walkway Beam					0.00078 (kip/in)		

Table A1-3. Loads Applied in Model of 110 ft Overhead Truss Sign Structure

	NWB	NWF	NWS		TGL	TGM	TGR
Supporting Frame Pipe	0.00047 (kip/in)		Below Truss	0.00063 (kip/in)			
			Above Truss	0.0012 (kip/in)			
Truss Chord	0.00070 (kip/in)	0.00064 (kip/in)			0.0027 (kip/in)		
Sign Beam	0.00022 (kip/in)						
Sign 1	0.000042 (ksi)						
Sign 2 and Sign 3	0.000043 (ksi)						
Walkway Beam					0.00078 (kip/in)		

Table A1-4. Loads Applied in Model of 137 ft Overhead Truss Sign Structure

	NWB	NWF	NWS		TGL	TGM	TGR
Supporting Frame Pipe	0.00047 (kip/in)		Below Truss	0.00064 (kip/in)			
			Above Truss	0.0012 (kip/in)			
Truss Chord	0.00070 (kip/in)	0.00058 (kip/in)			0.0027 (kip/in)		
Sign Beam	0.00022 (kip/in)						
Sign 1, 3, and 4	0.000040 (ksi)						
Sign 5	0.000041 (ksi)						
Sign 6	0.000042 (ksi)						
Sign 2	0.000043 (ksi)						
Walkway Beam					0.00078 (kip/in)		

APPENDIX A2 Example Calculation of Fatigue Load

Natural Wind Gust

$$P_{NW} = 5.2C_dI_F \quad \text{(Equation 3)}$$

Truck Induced Gust

$$P_{TG} = 18.8C_dI_F \quad \text{(Equation 4)}$$

Where,

C_d = Drag coefficient

I_F = Fatigue importance factor

$C_d = 1.2$ for all pipes

$C_d = 1.19$ for 3000 mm (118 in.) tall panel

$C_d = 1.14$ for 3450 mm (136 in.) tall panel

$C_d = 1.7$ for sign beam and walkway Beam

$I_F = 1.0$ for all

Natural Wind Gust

Calculate wind pressure

For truss pipes and supporting frame pipes

$$P_{NW} = 5.2 \times 1.2 \times 1.0 = 6.24 \text{ psf} = 4.33 \times 10^{-5} \text{ ksi}$$

For sign panel

$$P_{NW} = 5.2 \times 1.19 \times 1.0 = 6.19 \text{ psf} = 4.30 \times 10^{-5} \text{ ksi}$$

$$P_{NW} = 5.2 \times 1.14 \times 1.0 = 5.93 \text{ psf} = 4.12 \times 10^{-5} \text{ ksi}$$

For sign beam

$$P_{NW} = 5.2 \times 1.7 \times 1.0 = 8.84 \text{ psf} = 6.14 \times 10^{-5} \text{ ksi}$$

Natural Wind Blowing from Back of Sign Structure

Supporting frame column pipe

Length: 753.5 cm (296.7 in.)

Diameter: 27.3 cm (10.75 in.)

$$P_{NW} = 6.24 \text{ psf} = 4.33 \times 10^{-5} \text{ ksi}$$

$$f_{NW,SFCP} = 4.33 \times 10^{-5} \times 10.75 = 0.00047 \text{ kip/in}$$

Truss chord pipe

Length: 1870 cm = 736.22 in.

Diameter: 21.9 cm = 8.625 in.

$$f_{NW,TCP} = 4.33 \times 10^{-5} \times 8.625 = 0.00038 \text{ kip/in}$$

Truss web vertical pipe

Length: 180 cm = 70.87 in.

Diameter: 10.2 cm = 4.02 in.

$$f_{NW,TWVP} = 4.33 \times 10^{-5} \times 4.02 = 0.00017 \text{ kip/in}$$

$$F_{NW,TWVP} = 0.00017 \times 70.87 = 0.012 \text{ kip}$$

Truss web diagonal pipe

Length: 254 cm = 100 in.

Diameter: 10.2 cm = 4.02 in.

$$f_{NW,TWVP} = 4.33 \times 10^{-5} \times 4.02 = 0.00017 \text{ kip/in}$$

$$F_{NW,TWVP} = 0.00017 \times 100 = 0.017 \text{ kip}$$

Number of truss web vertical pipe projected to vertical plane: 11

Number of truss web diagonal pipe projected to vertical plane: 20

Total load on truss web pipes

$$F_{NW,TWP} = 0.012 \times 11 + 0.017 \times 20 = 0.48 \text{ kip}$$

Each truss chord take,

$$F_{NW,TWP/TC} = \frac{0.48}{2} = 0.24 \text{ kip}$$

Length of chord between the first and the last truss web pipe: 1850 cm (728.35 in.)

Convert to line load,

$$f_{NW,TWP/TC} = \frac{0.24}{728.35} = 0.00033 \text{ kip/in}$$

$$f_{NW,TC} = f_{NW,TCP} + f_{NW,TWP/TC} = 0.00038 + 0.00033 = 0.00071 \text{ kip/in}$$

Sign Beam

$$f_{NW,SB} = 6.14 \times 10^{-5} \times 3.5 = 0.00022 \text{ kip/in}$$

Natural Wind Blowing from Side of Sign Structure

Supporting frame column pipe

$$f_{NW,SFCP} = 4.33 \times 10^{-5} \times 10.75 = 0.00047 \text{ kip/in}$$

Load distributed from truss pipes

Total length

$$L_T = 4 \times 180 + 2 \times 254.56 = 1229.12 \text{ cm} = 483.91 \text{ in}$$

Total area

$$A_T = 483.91 \times 4.02 = 1945.32 \text{ in}^2$$

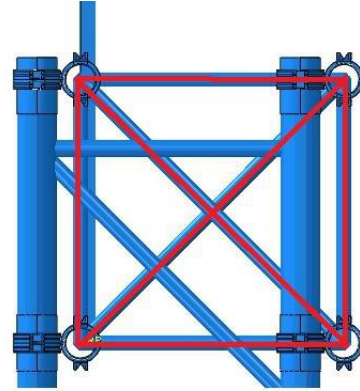
Total wind load

$$F_T = 1945.32 \times 4.33 \times 10^{-5} = 0.084 \text{ kip}$$

Distributed as line load

$$f_T = \frac{0.084}{70.87 \times 2} = 0.0006 \text{ kip/in}$$

Applied to the top portion of supporting frame



Load distributed from supporting frame brace pipes

Total length

$$L_T = 180 \times 2 + 254.56 + 247.93 \times 3 = 1358.35 \text{ cm} = 534.78 \text{ in}$$

Diameter: 11.4 cm = 4.49 in

Total area

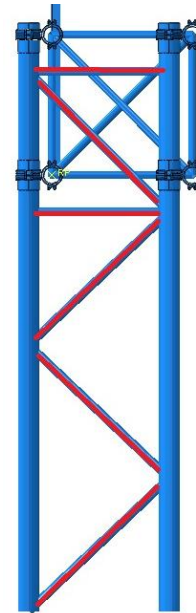
$$A_T = 534.78 \times 4.49 = 2401.16 \text{ in}^2$$

Total wind load

$$F_T = 2401.16 \times 4.33 \times 10^{-5} = 0.104 \text{ kip}$$

Distributed as line load

$$f_T = \frac{0.104}{290.74} = 0.00018 \text{ kip/in}$$



Total line load on supporting frame

$$f_{NW,SFT,B} = 0.00047 + 0.00018 = 0.00065 \text{ kip/in (Bottom Portion)}$$

$$f_{NW,SFT,T} = 0.00047 + 0.00018 + 0.0006 = 0.0013 \text{ kip/in (Top Portion)}$$

Truck-Induced Gust

Calculate wind pressure

Truss Pipes

$$P_{TG} = 18.8 \times 1.2 \times 1.0 = 22.56 \text{ psf} = 0.000157 \text{ ksi}$$

Calculate total truck-induced gust load applied on truss pipes

Total area of truss pipes subjected to truck-induced gust

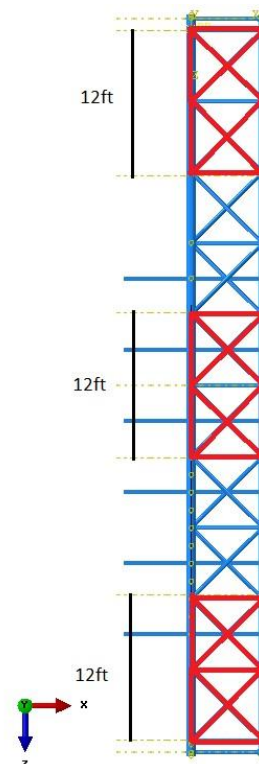
2×12ft truss chords, 3 vertical web pipes, and 4 diagonal web pip

$$A_{TP} = 365.76 \times 21.9 \times 2 + 180 \times 10.2 \times 3 + 254 \times 10.2 \times 4$$

$$= 31891.49 \text{ cm}^2 = 4943.19 \text{ in}^2$$

Total load on truss pipes

$$T_{TP} = 4943.19 \times 0.000157 = 0.78 \text{ kip}$$



Line load applied on truss chord

$$= \frac{\text{Loads on truss chords and web pipes within 12 ft}}{\text{Length of two chords}}$$

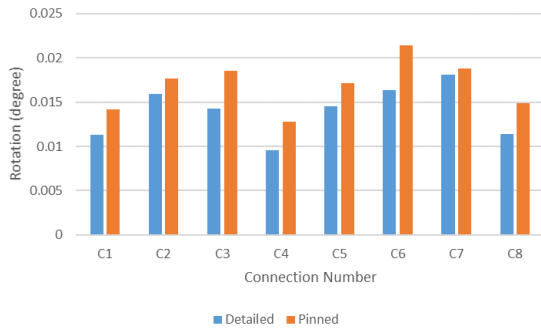
$$f_{TG,TP} = \frac{0.78}{12 \times 12 \times 2} = 0.0027 \text{ kip/in}$$

Walkway beam

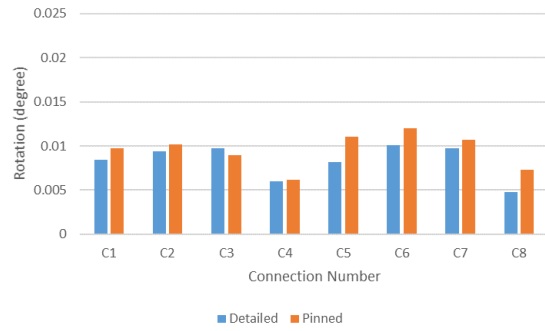
$$P_{TG} = 18.8 \times 1.7 \times 1.0 = 31.96 \text{ psf} = 0.000222 \text{ ksi}$$

$$f_{TG,WB} = 0.000222 \times 3.5 = 0.00078 \text{ kip/in}$$

APPENDIX A3 Connection Rotations in FE Models

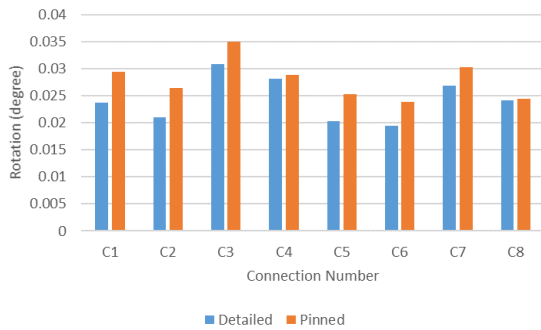


(a) Out-of-Plane Rotation

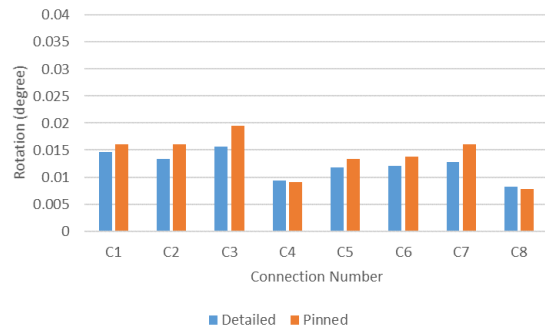


(b) In-Plane Rotation

Figure A3-1. Connection Rotations of 60 ft Sign Structure for Load Mode of Wind Blow from Back Side of Sign Structure

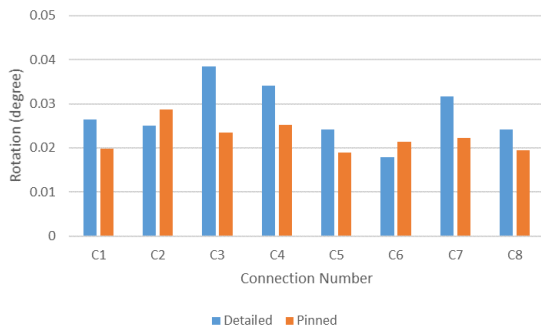


(a) Out-of-Plane Rotation

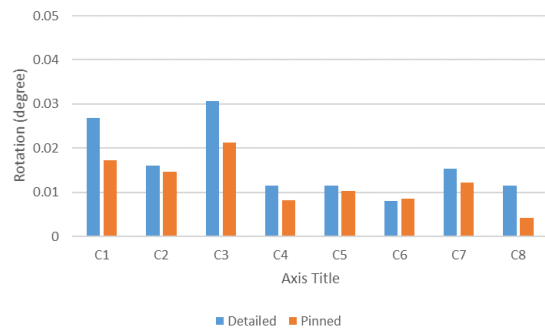


(b) In-Plane Rotation

Figure A3-2. Connection Rotations of 83 ft Sign Structure for Load Mode of Wind Blow from Back Side of Sign Structure

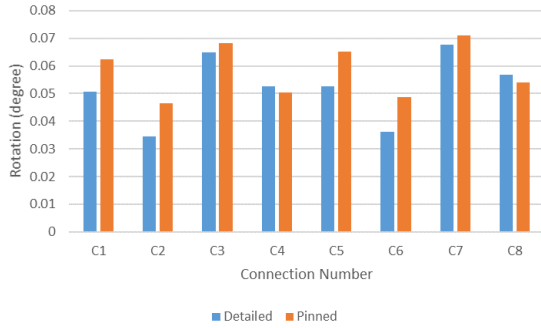


(a) Out-of-Plane Rotation

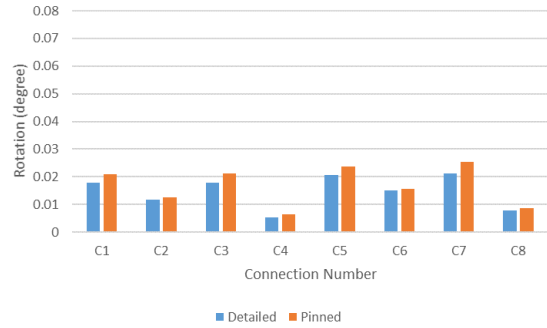


(b) In-Plane Rotation

Figure A3-3. Connection Rotations of 110 ft Sign Structure for Load Mode of Wind Blow from Back Side of Sign Structure



(a) Out-of-Plane Rotation



(b) In-Plane Rotation

Figure A3-4. Connection Rotations of 137 ft Sign Structure for Load Mode of Wind Blow from Back Side of Sign Structure

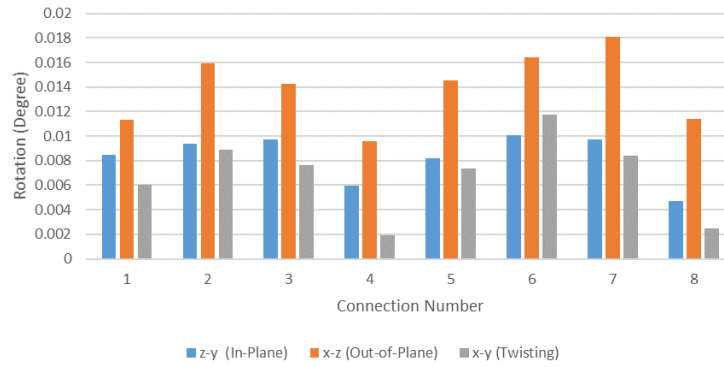


Figure A3-5. In-Plane, Out-of-Plane, and Twisting of Connection for 60 ft Detailed Model in Load Mode of Wind Blow from Back Side of Sign Structure

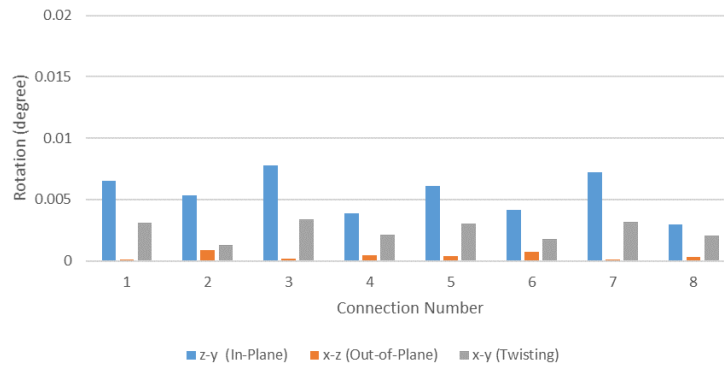


Figure A3-6. In-Plane, Out-of-Plane, and Twisting of Connection for 60 ft Detailed Model in Load Mode of Truck-Induced Gust Applied at Middle 12 ft

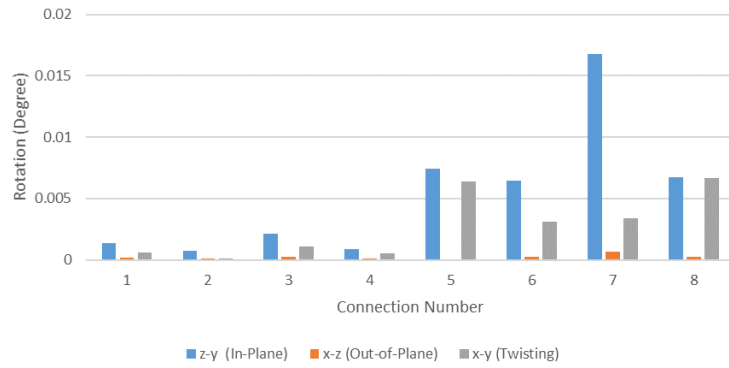


Figure A3-7. In-Plane, Out-of-Plane, and Twisting of Connection for 60 ft Detailed Model in Load Mode of Truck-Induced Gust Applied at Middle 12 ft

APPENDIX A4 Moment Diagrams of 60 ft Sign Structure

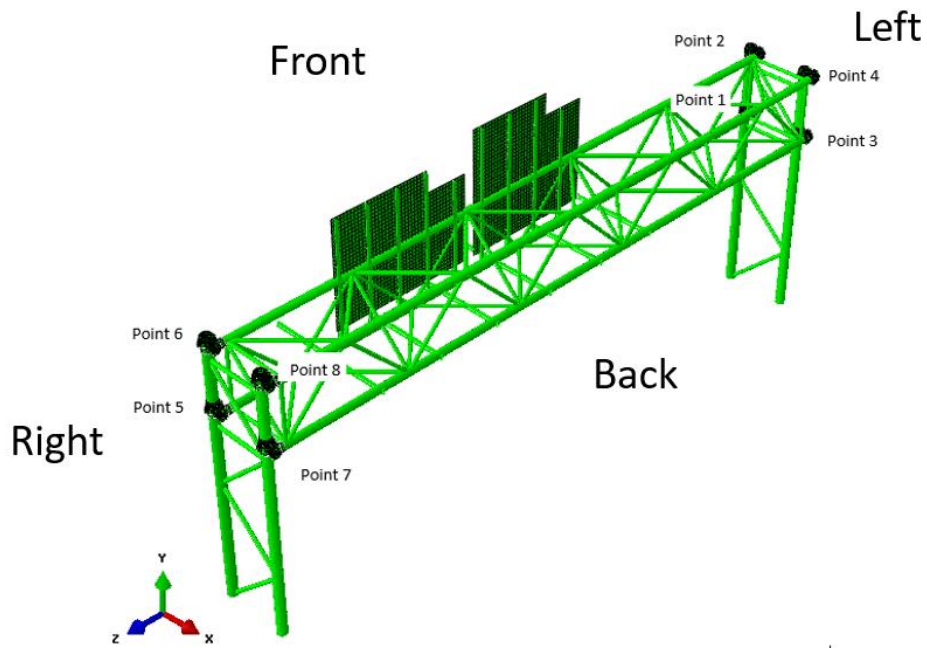


Figure A4-1 Label of Truss Chord to Support Frame Connection

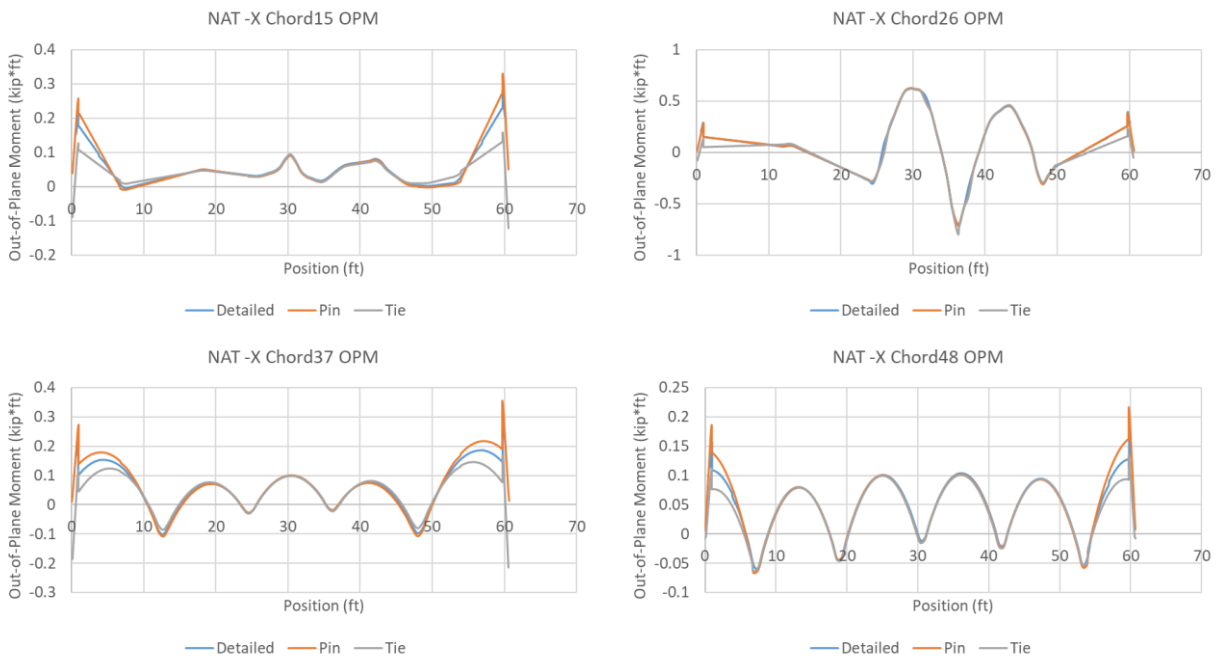


Figure A4-2 Out-of-Plane Moment Diagram for Natural Wind Blow from Back Side of Sign Structure

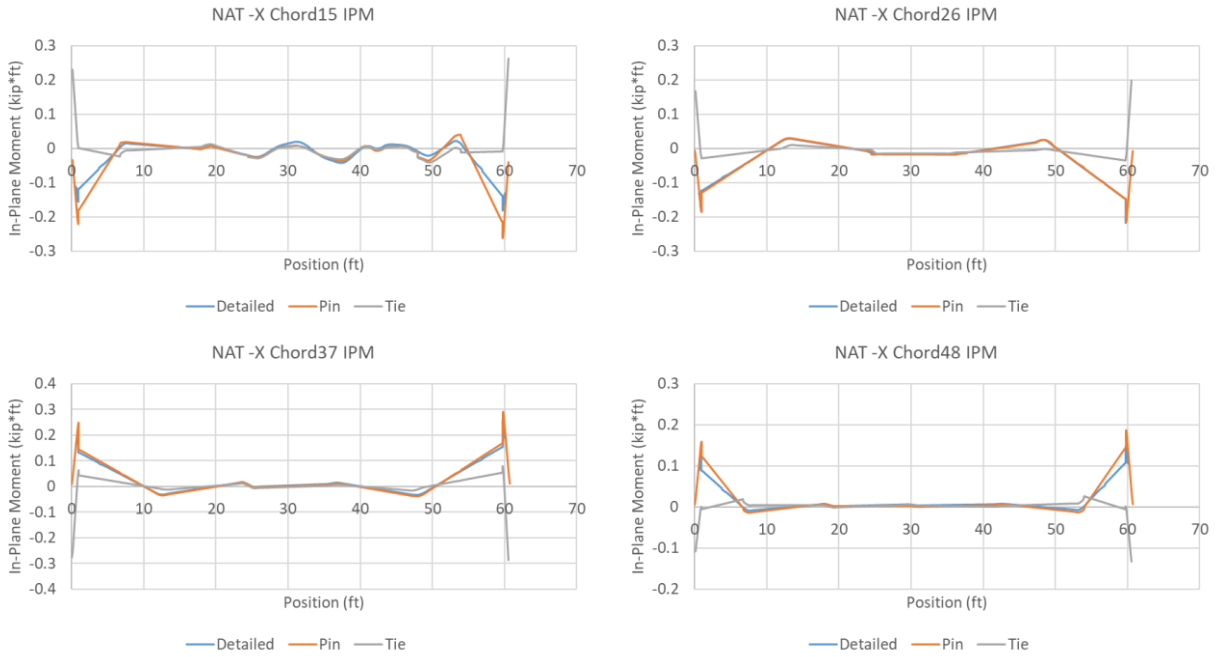


Figure A4-3 In-Plane Moment Diagram for Natural Wind Blow from Back Side of Sign Structure

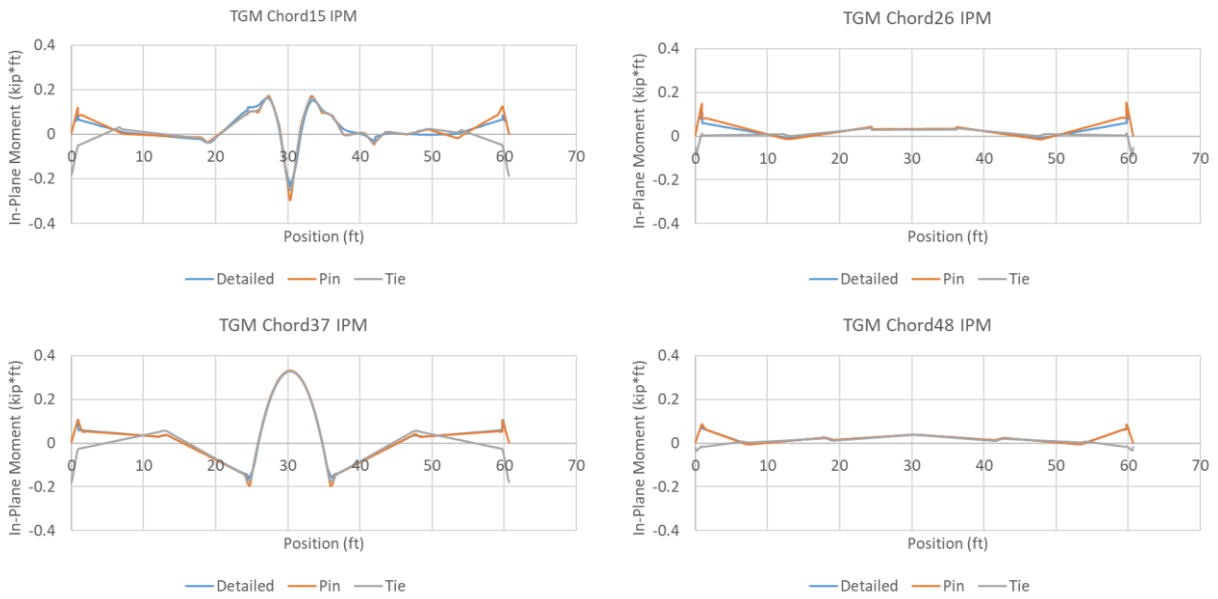


Figure A4-4 In-Plane Moment Diagram for Truck-Induced Gust Applied at Middle 12 ft

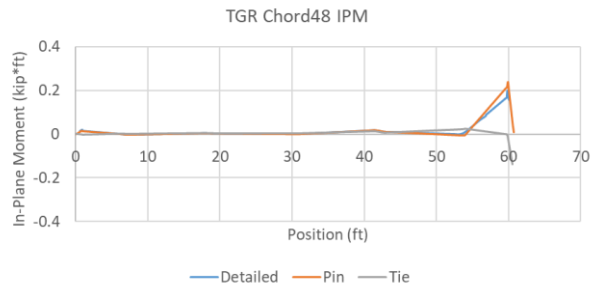
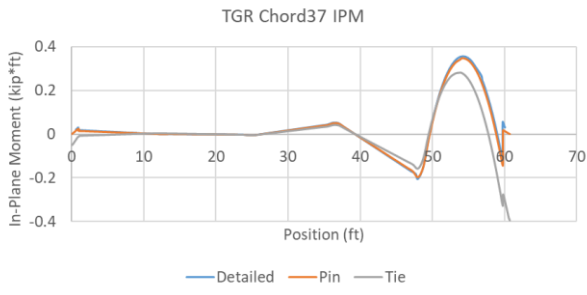
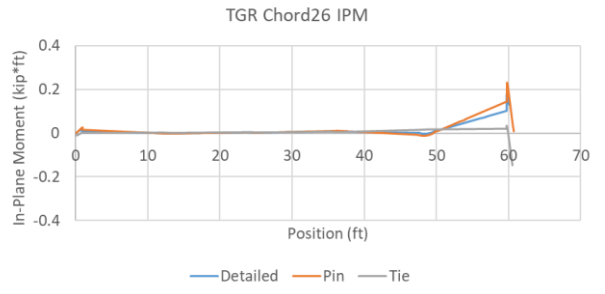
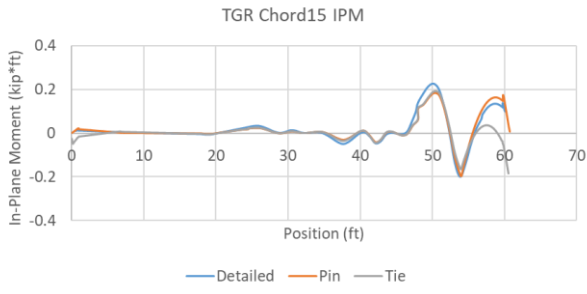


Figure A4-5 In-Plane Moment Diagram for Truck-Induced Gust Applied at Right 12 ft